ANALYSIS OF NON-CONFORMING DPG METHODS USING FRACTIONAL NORMS

C. Bacuta^a, L. Demkowicz^b, J. Mora Paz^b and Ch. Xenophontos^c

^aDepartment of Mathematics, University of Delaware
 ^bOden Institute, The University of Texas at Austin
 ^cDepartment of Mathematics and Statistics, University of Cyprus

Abstract

The work is concerned with two problems: a) analysis of a DPG method set up in fractional energy spaces, b) use of the results to analyze a non-conforming version of the DPG method for general, polyhedral meshes. We use the ultraweak variational formulation for the model Laplace equation. The theoretical estimates are supported with 3D numerical experiments.

1 Introduction

Model problem. The presented work is concerned with the analysis of a non-conforming version of the *Discontinuous Petrov-Galerkin (DPG) Method with Optimal Test Functions* based on the *Ultraweak (UW) variational formulation*. We shall focus on the model Poisson problem,

$$\begin{cases}
-\Delta u &= f & \text{in } \Omega \\
u &= 0 & \text{on } \Gamma
\end{cases}$$

where $\Omega \subset \mathbb{R}^N$ is a Lipschitz domain with boundary Γ . The UW formulation derives from the equivalent system of first order equations,

$$\begin{cases} \sigma - \nabla u &= 0 & \text{in } \Omega \\ -\text{div } \sigma &= f & \text{in } \Omega \\ u &= 0 & \text{on } \Gamma \end{cases}$$

which can be represented concisely in the operator form,

$$Au = f$$
.

Here $u := (\sigma, u)$ is a group variable, f = (0, f), and

$$Au = A(\sigma, u) = (\sigma - \nabla u, -\operatorname{div} \sigma).$$

More precisely,

$$A: L^2(\Omega) \supset D(A) \to L^2(\Omega)$$

is a closed operator with

$$D(A):=\{(\sigma,u)\in\mathsf{L}^2(\Omega)\,;\,A(\sigma,u)\in\mathsf{L}^2(\Omega),\,u=0\text{ on }\Gamma\}=H(\mathrm{div},\Omega)\times H^1_0(\Omega)\,,$$

where $L^2(\Omega) := L^2(\Omega)^N \times L^2(\Omega)$. The UW variational formulation is obtained by multiplying both equations with test functions τ, v and integrating by parts *both* equations. We obtain,

$$\begin{cases}
 u \in L^2(\Omega) \\
 (u, A^*v) = (f, v) \quad v \in D(A^*).
\end{cases}$$
(1.1)

Here A^* is the L²-adjoint of operator A,

$$A^* : \mathsf{L}^2(\Omega) \supset D(A^*) \to \mathsf{L}^2(\Omega)$$

$$A^*\mathsf{v} = A(\tau, v) = (\tau + \nabla v, \operatorname{div} \tau) \in \mathsf{L}^2(\Omega)$$

$$D(A^*) = D(A).$$

The *broken UW formulation* is obtained by testing with test functions from a larger space of *broken* test functions $V(\mathcal{T}_h) := H(\operatorname{div}, \mathcal{T}_h) \times H^1(\mathcal{T}_h)$. This necessitates introducing additional unknowns - the Lagrange multipliers, called *traces*,

$$\begin{cases}
\mathbf{u} \in \mathsf{L}^{2}(\Omega), \ \hat{\mathbf{u}} := \widehat{(\sigma \cdot n}, \hat{u}) \in H^{-1/2}(\Gamma_{h}) \times \widetilde{H}^{1/2}(\Gamma_{h}) \\
(\mathbf{u}, A_{h}^{*} \mathbf{v}) - \langle \hat{\mathbf{u}}, \mathbf{v} \rangle_{\Gamma_{h}} = (\mathsf{f}, \mathsf{v}) \quad \mathbf{v} \in V(\mathcal{T}_{h}).
\end{cases}$$
(1.2)

Here \mathcal{T}_h denotes a partition of the domain into finite elements, whose set of interfaces (or skeleton) is Γ_h and

$$\langle \hat{\mathbf{u}}, \mathbf{v} \rangle_{\Gamma_h} = \sum_{K \in \mathcal{T}_h} \left[\langle \widehat{\sigma \cdot n}, v \rangle_{\partial K} + \langle \hat{u}, \tau \cdot n \rangle_{\partial K} \right] \,.$$

Trace $\widehat{\sigma \cdot n}$ is defined by taking a function from $H(\operatorname{div},\Omega)$, restricting it to each element $K \in \mathcal{T}_h$, and taking its normal trace on element boundary ∂K . Similarly, trace \widehat{u} is obtained by taking a function from $H_0^1(\Omega)$, restricting it to each element K, and taking its trace on ∂K . The "tilde" symbol hides boundary condition on trace \widehat{u} ,

$$\tilde{H}^{1/2}(\Gamma_h) := \{\hat{u} \in H^{1/2}(\Gamma_h) \, : \, \hat{u} = 0 \text{ on } \Gamma\} \, .$$

It has been shown in [12] that problem (1.2) is well-posed.

The broken UW formulation is perhaps the least demanding formulation in terms of global conformity. The L^2 space is discretized with discontinuous functions, and so are the broken test spaces. The trace space $H^{-1/2}(\Gamma_h)$ is discretized with traces of Raviart-Thomas elements, i.e. with discontinuous functions over faces e in the mesh skeleton Γ_h . Only the discretization of \hat{u} , done with traces of H^1 -conforming elements, requires a global continuity over the element faces.

The numerical approximation to the solution of (1.2) implies a non-symmetric functional setting and solving the question if the discrete version of the problem is well-posed. To this end, the DPG finite element methodology, explained next, offers a framework that may solve this model problem, and any other variational problem that fits into the abstract setting that we now present.

DPG: Discontinuous Petrov-Galerkin with optimal test functions Suppose that we have the following abstract variational problem: find $\mathfrak{u} \in \mathscr{U}$ such that

$$b(\mathfrak{u},\mathfrak{v}) = \ell(\mathfrak{v}) \quad \forall \mathfrak{v} \in \mathscr{V}, \tag{1.3}$$

where both trial space $\mathscr U$ and test space $\mathscr V$ are real Hilbert spaces, $\ell \in \mathscr V'$, and $b(\cdot,\cdot):\mathscr U \times \mathscr V \to \mathbb R$ is a bilinear continuous functional, with continuity constant M, that satisfies the inf-sup condition

$$\inf_{\mathfrak{u}\in\mathscr{U}}\sup_{\mathfrak{v}\in\mathscr{V}}\frac{|b(\mathfrak{u},\mathfrak{v})|}{\|\mathfrak{u}\|_{\mathscr{U}}\|\mathfrak{v}\|_{\mathscr{V}}}=\gamma>0. \tag{1.4}$$

The energy norm $\|\cdot\|_E$ on \mathscr{U} is defined as follows:

$$\|\mathfrak{u}\|_{E} = \sup_{\mathfrak{v} \in \mathscr{V}} \frac{|b(\mathfrak{u}, \mathfrak{v})|}{\|\mathfrak{v}\|_{\mathscr{V}}}.$$
(1.5)

Let $\mathscr{B}:\mathscr{U}\to\mathscr{V}'$ be a linear operator defined by $\mathscr{B}\mathfrak{u}:=b(\mathfrak{u},\cdot)$; then (1.5) is equivalent to

$$\|\mathfrak{u}\|_{E} = \sup_{\mathfrak{v} \in \mathscr{V}} \frac{|\langle \mathscr{B}\mathfrak{u}, \mathfrak{v} \rangle|}{\|\mathfrak{v}\|_{\mathscr{V}}} = \|\mathscr{B}\mathfrak{u}\|_{\mathscr{V}'}. \tag{1.6}$$

The ideal DPG method: The ideal DPG method is a minimum residual FE method that delivers the best approximation error in the energy norm (1.5). This is equivalent to minimizing the residual in the dual test space norm (by virtue of (1.6)). More precisely, given a discrete trial subspace $\mathcal{U}^h \subset \mathcal{U}$ with dimension N_h , the ideal DPG solution $\mathfrak{u}_h \in \mathcal{U}^h$ satisfies

$$\|\mathfrak{u} - \mathfrak{u}_h\|_E = \inf_{\mathfrak{w}_h \in \mathscr{U}^h} \|\mathfrak{u} - \mathfrak{w}_h\|_E = \inf_{\mathfrak{w}_h \in \mathscr{U}^h} \|\mathscr{B}(\mathfrak{u} - \mathfrak{w}_h)\|_{\mathscr{V}'} = \inf_{\mathfrak{w}_h \in \mathscr{U}^h} \|\ell - \mathscr{B}\mathfrak{w}_h\|_{\mathscr{V}'}. \tag{1.7}$$

where $\mathfrak{u} \in \mathscr{U}$ is the exact solution to (1.3). Now, let $\mathscr{R}_{\mathscr{V}} : \mathscr{V} \to \mathscr{V}'$ be the Riesz map of \mathscr{V} associated with norm $\|\cdot\|_{\mathscr{V}}$. Then,

$$\|\mathfrak{u} - \mathfrak{u}_h\|_E = \inf_{\mathfrak{w}_h \in \mathscr{U}^h} \|\mathscr{R}_{\mathscr{V}}^{-1}(\ell - \mathscr{B}\mathfrak{w}_h)\|_{\mathscr{V}}. \tag{1.8}$$

By working out the minimization problem in (1.8), the ideal DPG corresponds to the following Petrov-Galerkin formulation [27]: find $\mathfrak{u}_h \in \mathcal{U}^h$ such that

$$b(\mathfrak{u}_h,\mathfrak{v}_h) = \ell(\mathfrak{v}_h) \quad \forall \mathfrak{v}_h \in \mathscr{V}^h := \mathbf{T}\mathscr{U}^h \subset \mathscr{V}, \tag{1.9}$$

where $\mathbf{T}: \mathcal{U} \to \mathcal{V}$ is the *trial-to-test* map, defined by $\mathbf{T} := \mathcal{R}_{\mathcal{V}}^{-1}\mathcal{B}$. The functions in \mathcal{V}^h are known as *optimal test functions* because they automatically grant discrete stability to this Petrov-Galerkin discretization. The following stability estimate holds for the solution of (1.9) [27]:

$$\|\mathfrak{u} - \mathfrak{u}_h\|_{\mathscr{U}} \le \frac{M}{\gamma_h} \inf_{\mathfrak{w}_h \in \mathscr{U}^h} \|\mathfrak{u} - \mathfrak{w}_h\|_{\mathscr{U}} \le \frac{M}{\gamma} \inf_{\mathfrak{w}_h \in \mathscr{U}^h} \|\mathfrak{u} - \mathfrak{w}_h\|_{\mathscr{U}}, \tag{1.10}$$

where $\gamma_h \ge \gamma$ is the discrete inf-sup constant of the bilinear functional b.

Remark 1 For our model problem, we can identify the ingredients of the ideal abstract DPG method as follows: \mathfrak{u} is the trial group variable $(\mathfrak{u}, \hat{\mathfrak{u}}) = (\sigma, u, \widehat{\sigma \cdot n}, \hat{u})$; \mathfrak{v} is the test group variable $\mathsf{v} = (\tau, v)$; the trial space is $\mathscr{U} = \mathsf{L}^2(\Omega) \times H^{-1/2}(\Gamma_h) \times \widetilde{H}^{1/2}(\Gamma_h)$, while the (broken) test space is $\mathscr{V} = H(\operatorname{div}, \mathcal{T}_h) \times H^1(\mathcal{T}_h)$; the bilinear functional $b(\mathfrak{u}, \mathfrak{v})$ and the linear operator $\ell(\mathfrak{v})$ are the left-hand side and right-hand side of the equation in (1.2), respectively. Constants M and γ are found in [26, 35].

 $\mathcal{D}PG$ in practice: Unless we are dealing with a very special test space, for which inverting its Riesz map $\mathscr{R}_{\mathscr{V}}$ is feasible, in general this problem is infinite-dimensional, so it is impossible to perform without some approximation. Hence we need to work with a finite-dimensional enriched test space $\mathscr{V}^r \subsetneq \mathscr{V}$ rather than with the whole space. The dimension of this space is $N_r \geq N_h$. To attain the so-called practical DPG method, the only required modification to (1.9) is to replace \mathbf{T} by its discrete counterpart $\mathbf{T}^r := (\mathscr{R}_{\mathscr{V}^r})^{-1} \iota^{\mathsf{T}} \mathscr{B}$, that maps trial functions into the enriched test space; here, $\mathscr{R}_{\mathscr{V}^r}$ is the Riesz map of \mathscr{V}^r and ι^{T} is the transpose of the inclusion $\iota : \mathscr{V}^r \to \mathscr{V}$.

We may now translate the formulation into an algebraic problem. Let's take a basis of \mathcal{V}^r , $\{\mathfrak{v}_k^r\}_{k=1}^{N_r}$; hence the *near-optimal* test functions $\{\mathfrak{v}_{i,\text{n-opt}}\}_{i=1}^{N_h}$ can be computed through

$$v_{i,\text{n-opt}} = \sum_{j,k=1}^{N_r} (\mathsf{B}^\mathsf{T})_{ij} (\mathsf{G}^{-1})_{jk} v_k \quad i = 1, ..., N_h,$$
(1.11)

where B is called the enriched stiffness matrix, and G is the Gram matrix of \mathcal{V}^r , defined by

$$\mathsf{B}_{ji} := b(\mathfrak{u}_i, \mathfrak{v}_j^r), \qquad \qquad \mathsf{G}_{kj} := (\mathfrak{v}_j^r, \mathfrak{v}_k^r)_{\mathscr{V}}$$

where $\{\mathfrak{u}_i\}_{i=1}^{N_h}$ is a basis for \mathscr{U}^h . Additionally, define the vector \mathfrak{l} by $\mathfrak{l}_k := \ell(\mathfrak{v}_k^r)$. If the numerical solution is written like $\mathfrak{u}^h = \sum \mathfrak{u}_i \mathsf{d}_i$, the coefficient vector d solves the discrete linear system

$$\mathsf{B}^{\mathsf{T}}\mathsf{G}^{-1}\mathsf{Bd} = \mathsf{B}^{\mathsf{T}}\mathsf{G}^{-1}\mathsf{l}. \tag{1.12}$$

In (1.12), let the left-hand side matrix be denoted $B^{n\text{-}\mathrm{opt}} = B^T G^{-1} B$, which is symmetric and positive definite, and the right-hand side vector by $l^{n\text{-}\mathrm{opt}} = B^T G^{-1} l$, where the n-opt superscript alludes to the near-optimal test functions being utilized. In short, the practical DPG solves the problem $B^{n\text{-}\mathrm{opt}} d = l^{n\text{-}\mathrm{opt}}$.

The stability of the ideal DPG method is carried over to the practical DPG method if there exists a linear operator $\Pi_F : \mathcal{V} \to \mathcal{V}^r$, hereinafter referred to as the Fortin operator, satisfying these conditions [35]:

$$\begin{cases}
b(\mathfrak{u}_h, \mathfrak{v} - \Pi_F \mathfrak{v}) = 0 & \forall \mathfrak{v} \in \mathcal{V}, \mathfrak{u}_h \in \mathcal{U}^h \text{ (orthogonality)} \\
\|\Pi_F \mathfrak{v}\|_{\mathscr{V}} \leq C_F \|\mathfrak{v}\|_{\mathscr{V}} & \forall \mathfrak{v} \in \mathscr{V} \text{ (continuity)}
\end{cases}$$
(1.13)

Using C_F , the continuity constant of Π_F in (1.13), the estimate (1.10) becomes

$$\|\mathfrak{u} - \mathfrak{u}_h\|_{\mathscr{U}} \le \frac{C_F M}{\gamma} \inf_{\mathfrak{w}_h} \|\mathfrak{u} - \mathfrak{w}_h\|_{\mathscr{U}}. \tag{1.14}$$

Remark 2 The abstract presentation above only yields a Petrov-Galerkin method with optimal test functions. The use of broken test functions is what gives DPG its *discontinuous* character. This type of test functions allows to compute B^{n-opt} locally and then assemble it into a global matrix, instead of assembling G globally and inverting it, which would be a much more expensive process than the actual discrete problem.

Polygonal and Polyhedral Finite Element methods. Numerical solutions of boundary value problems (BVPs) with meshes of general polytopes have raised great attention over the last two decades, although the first methods were proposed much earlier by Wachspress [52]. The latter introduced rational barycentric coordinates, which formed a finite element basis over convex polygons, leading to a conforming finite element (FE) method with a new type of element. We can regard this as the first conforming polygonal FE method (PFEM), in which a stiffness matrix is computed as in the classical Galerkin formulation, and the theory of approximation is based on the fact that their discrete spaces fulfill some type of global continuity which makes them a subspace of the corresponding infinite-dimensional trial or test space. Precisely here lies a major challenge when working with polytopal elements, as coming up with a conforming finite basis for arbitrary polygonal or polyhedral meshes requires working with non-polynomial functions.

Other generalized barycentric coordinates on polygons, have been used in this FE approach, enabling the use of non-convex elements as well. Within the family of PFEM with generalized barycentric coordinates, we can find methods working with harmonic coordinates [6], entropy coordinates, mean-value coordinates and others [41]. Applications of such methods are known in elasticity, optimization, crack propagation, pervasive fracture, etc. [48, 15, 50, 47, 7]. Research on numerical integration on polytopes, adaptive refinementes with such methods, and higher order spaces has also received attention [49, 42, 16, 46, 34].

However, besides PFEM a growing collection of numerical methods that use general polytopes to discretize is now available, and many are built upon principles other than conforming FE methods.

A related class of finite difference (FD) methods, called the mimetic finite difference (MFD) methods, but based on mimicking differential operators in a discrete setting, has also been extended to polytopal grids successfully [38, 9, 9]. From the ideas of MFD, a new method with a growing acceptance nowadays has been developed: the virtual element method (VEM). The method avoids explicit construction of shape functions that are conforming to polytopal meshes, but instead tailors spaces that virtually comply with conformity. The virtual shape functions are not accessed directly, but only through their projection onto polynomial spaces. VEM has been applied to a large number of applications and has generated high order approximations of equations of a very diverse nature. Additionally, VEM works with elements with very relaxes regularity assumptions, which makes it really versatile. It does require, however, a stabilization term that is problem-dependent. It cannot either deliver its real solution (it is virtual) but only a polynomial projection of it. For representative developments of the subject, see [3, 21, 4, 10, 20, 13, 14, 33, 5, 19]. Other methods include versions of Finite Volume (FV) methods, Discontinuous Galerkin FE methods, or similar approaches that, because of their low-regularity requirements or non-conforming character, can be extended

to elements of arbitrary shape [45, 11, 43, 17, 30]. We fail to mention a number of additional techniques that altogether illustrate that polytopal meshes has become a "hot subject" in numerical analysis.

PolyDPG. DPG has been recently introduced into the family of polygonal methods by Vaziri, Fuentes, Mora and Demkowicz [51], who have labeled their proposed methodology as *PolyDPG*. In 2D, the extension of DPG to polygonal elements has been enabled by the *ultraweak variational formulation* and *broken test spaces*. These two features have allowed for use of discontinuous trial and test functions inside the elements, leaving the connectivity throughout the domain handled only by trace variables defined on the mesh skeleton, which in 2D is simply the union of line segments. The issue of finding a basis of globally continuous basis functions for polygons has thus been avoided. A convergence analysis of the method delivered an optimal error estimate. The theoretical findings have been verified numerically. The highlights of the two-dimensional version of PolyDPG, in contrast to other methods, are that it is a high-order and stable polygonal finite element method, whose ultraweak-conforming discrete spaces are constructed with polynomials only.

Also in 3D, a conforming discretization of trace \hat{u} ought to consist of basis functions that are globally continuous throughout the entire mesh skeleton, which is the union of all the faces. Since traditional elements (tetrahedra, hexahedra, prisms and pyramids) possess triangular and quadrilateral faces only, it is indeed possible to build such discrete spaces (using for instance traces of conforming spaces derived for such element types, such as those in [32]). Even if the element is a more general polyhedron, but with all its faces being triangular or quadrilateral, it is possible to have a piecewise polynomial conforming discrete space for approximating \hat{u} . If this is the case, we could show the convergence of the practical DPG for (1.2) following a procedure similar to the 2D case [51], whenever we have analogous assumptions regarding element shape and Fortin operators.

For general polygonal faces, obtaining such a conforming discrete subspace is not possible with facewise polynomials only (it is a problem as difficult as getting a globally continuous basis for 2D polygonal meshes). A discontinuous polynomial basis is therefore a practical but *non-conforming* way to discretize the subspace for this unknown.

For this reason, we must study the effect on the stability and approximability of the PolyDPG method when choosing a discontinuous basis for the trace \hat{u} . In the literature there are results about this situation in DPG when dealing with standard elements, but when the element is an arbitrary polyhedron (which has any number of polygonal faces) the analysis turns more complicated, starting with the fact that there is no unique reference element or unique reference face, so that we need to argue that the error estimates can be independent of the element shape.

Next, we review the main ideas and conclusions from previous work on non-conforming DPG and remark which points are of most interest to us in our analysis.

Existing analysis of non-conforming DPG method. In an early preprint paper on analysis of the DPG method, Demkowicz and Gopalakrishnan presented 2D computations using discontinuous polynomials for

the discretization of all traces, making one of the variables non-conforming. Even though this could be perceived as a "variational crime", because the analysis was relying on conformity, the numerical results were satisfactory [26]. Noticing this finding, Heuer, Karkulik and Sayas first studied the convergence of a DPG method with discontinuous traces on simplicial meshes [36]. Such analysis delivered the following conclusions:

- 1. It is possible to furnish the trial space with a weaker norm, and the test space with a stronger norm, such that the continuous problem remains well-posed and the discretization with discontinuous traces gives rise to a conforming DPG method (with respect to the new functional setting).
- 2. If we wish to keep our original trial norm to measure the error, the analysis shows quasi-optimal convergence for the main unknown only (cf. [36, Theorem 1 and Corollary 2]), while if the trial norm is the *energy norm*, all variables are quasi-optimally controlled by the best approximation error (cf. [36, Remark 9]).
- 3. The computational implementation is invariant to the choice of the norms mentioned above, since we can keep computing DPG's optimal test functions with the Riesz operator corresponding to the original test norm. In other words, the new functional setting is a theoretical artifice necessary for proving convergence, but the practical DPG implementation of (1.12) remains as if we had the original test norm.

Below, we use their argument to transfer our results in fractional-Sobolev test norms to the integral-Sobolev (original) test norm.

Another relevant development in non-conforming DPG is that by Ernesti and Wieners on space-time DPG for linear wave problems [31]. There, in what the authors call a "simplified DPG method", the discretization of the traces is made independently over each facet of the tensor-product space-time cells, without enforcing continuity. For the sake of the analysis, it is assumed that there exists a "reconstruction" space, which is a subspace of the local field space such that its traces deliver the same linear system as the non-conforming space. Following this assumption, a new discrete norm is proposed and this allows to transfer the convergence result for a conforming DPG method (cf. [31, Theorem 5.2]) to the non-conforming scenario (cf. [31, Theorem 6.1]). As in the other cited work, here this new subspace is merely virtual, and never used in computations.

Goal, scope and organization of this paper. The present paper is concerned with the stability analysis and a-priori error estimate for a non-conforming version of both the ideal and practical DPG methods for the Poisson problem, in which the discretization of trace \hat{u} is done with *discontinuous* polynomials. The rationale behind this endeavor is that, unlike $H^{1/2}$, the fractional spaces that we are considering below contain discontinuous piecewise polynomials, thus this discretization is conforming with respect to the fractional spaces, and the Babuška-Necas theorem provides the stability for this case. Given the complexity of

a computational implementation of fractional norms, all numerical results reported below correspond to the original functional setting, which can be interpreted as the limit case of the fractional setting considered in our theoretical framework.

In Section 2, we start by analyzing the infinite-dimensional scenario of the Poisson model problem formulated in fractional spaces. After introducing the fractional Sobolev spaces and norms, we show that the classical variational formulation is well-posed, which in turn helps proving that the ultraweak variational formulation is well-posed too, as derived in Section 3. Once there, in Section 4 we begin the analysis with broken test spaces and localization of fractional norms, to get to the first major results: the inf-sup condition of the broken ultraweak formulation, and the stability for the ideal DPG with fractional norms (cf. Theorems 2 and 3).

Section 5 deals with the implications of the present analysis on the practical non-conforming DPG. By stating and checking four assumptions (one of them deeplier elaborated in Appendix A), we get the discrete stability for a DPG method that is computationally implemented with the original integral Sobolev norms, but controlling the error in the weaker fractional norms. This is followed by the analysis on approximability of the discrete trace spaces (Section 6). The ultimate a-priori error estimates herein developed are found in Section 7,

A collection of numerical results of PolyDPG with discontinuous discretization of \hat{u} is presented in section 8, showing a diverse group of polyhedral meshes on which the method works, delivering convergence rates similar to the theoretical ones for some or all the unknowns. The conclusions of the paper are included in Section 9.

2 Classical Variational Formulation

Fractional Sobolev spaces. In this section we review the equivalence of different definitions of fractional Sobolev spaces $H^s(\Omega)$. Most of these equivalences can be found in [23]. We assume that Ω is at least a Lipschitz domain.

Minimum energy extension norm versus the Slobodeckij norm. Let $\Omega \subset \mathbb{R}^N$ be an arbitrary domain and assume $s \in (0, 1)$. We assume that the definition of $H^s(\mathbb{R}^N)$ is the standard one, see [23]. Then, the norm on $H^s(\Omega)$ is the minimum energy extension norm

$$||u||_{H^{s}(\Omega)}^{2} = \min\left\{||U||_{H^{s}(\mathbb{R}^{N})}^{2} : U|_{\Omega} = u\right\}.$$
(2.15)

The Slobodeckij seminorm is defined by

$$|u|_{s,\Omega}^2 := \int_{\Omega} \int_{\Omega} \frac{|u(x) - u(y)|^2}{|x - y|^{N+2s}} dx dy.$$

For $s \in (0, 1/2)$ the Slobodeckij (rescaled) norm can be defined by

$$||u||_{s,\Omega}^2 := ||u||_{L^2(\Omega)}^2 + c(s)|u|_{s,\Omega}^2, \tag{2.16}$$

where c(s) > 0 and c(s) = O(s) when $s \to 0$.

It is known, see e.g. [23, Section 3.2], that if a continuous linear extension from $(H^s(\Omega), \|\cdot\|_{s,\Omega}^2)$ to $H^s(\mathbb{R}^N)$ exists, then the two norms (2.15) and (2.16) are equivalent and define the same space $H^s(\Omega)$.

Interpolation and Spectral norm characterization We assume again that $\Omega \subset \mathbb{R}^N$ is an arbitrary (smooth) domain and let $s \in (0, 1)$. One can define $H^s(\Omega)$ using the real method of interpolation, see e.g. [40, Section 9.1], by;

$$H^s(\Omega) := \left[H^1(\Omega), L^2(\Omega) \right]_{1-s}. \tag{2.17}$$

According to [40, Theorem 9.2], the interpolation norm and the *minimum energy extension norm* are equivalent.

The space $H_0^s(\Omega)$, interpolation and spectral norm characterization For $s \in (0, \infty)$ we can define the space $H_0^s(\Omega)$ by

$$H_0^s(\Omega) = \overline{C_0^\infty(\Omega)}^{H^s(\Omega)}.$$

It is known that for $s \in (0, 1)$ the space can be also be characterized as

$$H_0^s(\Omega) = [H_0^1(\Omega), L^2(\Omega)]_{1-s},$$
 (2.18)

 $H_0^s(\Omega) = H^s(\Omega)$ for 0 < s < 1/2, and $H_0^s(\Omega)$ is a proper closed subspace of $H^s(\Omega)$ for 1/2 < s < 1

Using the interpolation characterization of $H_0^s(\Omega)$ we can also describe its norm using the spectrum of the Laplace operator. More precisely, we consider the operator

 $-\Delta:D(-\Delta)\subset H^1_0(\Omega)\subset L^2(\Omega)\to L^2(\Omega),$ where $D(-\Delta):=\{u\in H^1_0(\Omega):\Delta u\in L^2(\Omega)\}.$ It is known that the spectrum of $-\Delta$ as an (unbounded) operator from $L^2(\Omega)$ to $L^2(\Omega)$ is discrete and depends only on the domain Ω . The eigenvalues λ_k and corresponding eigenfunctions e_k are defined by the problem: Find $e_k\in H^1_0(\Omega)$ s.t.

$$\begin{cases}
-\Delta e_k &= \lambda_k e_k & \text{in } \Omega \\
e_k &= 0 & \text{on } \Gamma
\end{cases}$$

It is also known that if the eigenvalues are ordered s.t. $0<\lambda_1\leq \lambda_2\leq \cdots \lambda_k, \cdots$, then

$$\lim_{k \to \infty} \lambda_k = +\infty,$$

and we can assume w.l.o.g., that $\{e_k\}_{k\geq 1}$ form an orthonormal basis for $L^2(\Omega)$. Then, for any $u\in L^2(\Omega)$,

$$u = \sum_{k=1}^{\infty} (u, e_k) e_k,$$

and, denoting $u_k := (u, e_k)$,

$$||u||_{L^2(\Omega)}^2 = \sum_{k=1}^{\infty} u_k^2. \tag{2.19}$$

For $u \in H^1_0(\Omega) \cap D(-\Delta)$, the expansion $u = \sum_{k=1}^\infty u_k e_k$ leads to

$$-\Delta u = \sum_{k=1}^{\infty} \lambda_k u_k e_k,$$

consequently,

$$||u||_{H_0^1(\Omega)}^2 = (\nabla u, \nabla u) = (-\Delta u, u) = \sum_{k=1}^{\infty} \lambda_k u_k^2.$$
 (2.20)

Using the interpolation definition (2.18) of the space $H_0^s(\Omega)$, and the norms on L^2 and H_0^1 given by (2.19) and (2.20), respectively, it is easy to see that

$$||u||_{H_0^s(\Omega)}^2 = c_s^{-2} \sum_{k=1}^{\infty} \lambda_k^s u_k^2, \tag{2.21}$$

where $c_s = \sqrt{\frac{2}{\pi} \sin \pi s}$, see e.g., the Appendix of [8].

As a direct consequence, for $\epsilon \in (0, 1/2)$ we have

$$||u||_{H_0^{1-\epsilon}(\Omega)}^2 = c_{\epsilon}^{-2} \sum_{k=1}^{\infty} \lambda_k^{1-\epsilon} u_k^2.$$
 (2.22)

This is because $c_{1-\epsilon} = \sqrt{\frac{2}{\pi}\sin\pi(1-\epsilon)} = c_{\epsilon}$.

If we assume that we have full regularity for the $-\Delta$ operator then the norm on $H^2(\Omega) \cap H^1_0(\Omega)$ is equivalent with $\|\Delta \cdot \|$ or

$$||u||_{H^2(\Omega)\cap H_0^1(\Omega)}^2 := (\Delta u, \Delta u) = \sum_{k=1}^{\infty} \lambda_k^2 u_k^2$$
(2.23)

Thus, for $s\in(0,\,1)$ the space $H_0^{1+s}(\Omega)$ can be also be characterized as

$$H_0^{1+s}(\Omega) = \left[H^2(\Omega)\cap H_0^1(\Omega), H_0^1(\Omega)\right]_{1-s},$$

Using this (interpolation) definition for $H_0^{1+s}(\Omega)$, and the norms on $H^2(\Omega) \cap H_0^1(\Omega)$ and $H_0^1(\Omega)$ given by (2.23) and (2.20), respectively, one can check, by estimating the K functional, that

$$||u||_{H_0^{1+\epsilon}(\Omega)}^2 = c_{\epsilon}^{-2} \sum_{k=1}^{\infty} \lambda_k^{1+\epsilon} u_k^2.$$
 (2.24)

Well-posedness of the classical variational formulation in fractional spaces. Given $\epsilon \in (0, 1/2)$ we consider the following variational formulation: Find u such that

$$\left\{ \begin{array}{ll} & u \in H^{1-\epsilon}(\Omega), \\ & (\nabla u, \nabla v) &= (f,v), \end{array} \right. \quad \text{for all } v \in H^{1+\epsilon}(\Omega).$$

Consider that the norms on $H_0^{1-\epsilon}(\Omega)$ and $H_0^{1+\epsilon}(\Omega)$ are given by (2.22) and (2.24), respectively.

Then, we can establish the following result.

Lemma 1

ı

The following estimate holds:

$$\sup_{v \in H_0^{1+\epsilon}(\Omega)} \frac{(\nabla u, \nabla v)}{\|v\|_{H_0^{1+\epsilon}(\Omega)}} = c_{\epsilon}^2 \|u\|_{H_0^{1-\epsilon}(\Omega)}.$$
(2.25)

Proof: Let $u = \sum_{k=1}^{\infty} u_k e_k \in H_0^{1-\epsilon}$ and $v = \sum_{k=1}^{\infty} v_k e_k \in H_0^{1+\epsilon}$. Then, using the Cauchy-Schwarz inequality,

$$(\nabla v, \nabla u) = (-\Delta v, u) = \sum_{k=1}^{\infty} \lambda_k u_k v_k = \sum_{k=1}^{\infty} \lambda_k^{\frac{1-\epsilon}{2}} u_k \lambda_k^{\frac{1+\epsilon}{2}} v_k$$

$$\leq \left(\sum_{k=1}^{\infty} \lambda_k^{1-\epsilon} u_k^2\right)^{1/2} \left(\sum_{k=1}^{\infty} \lambda_k^{1+\epsilon} v_k^2\right)^{1/2}$$

$$= c_{\epsilon} \|u\|_{H_0^{1-\epsilon}(\Omega)} c_{\epsilon} \|v\|_{H_0^{1+\epsilon}(\Omega)}.$$

$$(2.26)$$

To prove the reverse inequality we fix $u=\sum_{k=1}^\infty u_k e_k\in H_0^{1-\epsilon}$ and define v_u by

$$v_u = \sum_{k=1}^{\infty} \lambda_k^{-\epsilon} u_k e_k.$$

One can immediately check that $v_u \in H_0^{1+\epsilon}(\Omega)$ and $\|v_u\|_{H_0^{1+\epsilon}(\Omega)} = \|u\|_{H_0^{1-\epsilon}(\Omega)}$. Then

$$\sup_{v \in H_0^{1+\epsilon}(\Omega)} \frac{(\nabla u, \nabla v)}{\|v\|_{H_0^{1+\epsilon}(\Omega)}} \geq \frac{(\nabla u, \nabla v_u)}{\|v_u\|_{H_0^{1+\epsilon}(\Omega)}} = \frac{\sum_{k=1}^\infty \lambda_k^{1-\epsilon} u_k^2}{\|u\|_{H_0^{1-\epsilon}(\Omega)}} = c_\epsilon^2 \|u\|_{H_0^{1-\epsilon}(\Omega)}.$$

NOTE: If we define the norm on the fractional spaces without c_{ϵ} the constant in the above Lemma is 1. Since for s>1/2 the L^2 component of the H^s norm is not essential we may decide to work with the spectral norm

$$||u||_{s,0}^2 := \sum_{k=1}^{\infty} \lambda_k^s u_k^2.$$

3 Ultraweak Variational Formulation

The well-posedness analysis of various variational formulations presented in [22] extends easily to fractional spaces. Let $s \in [0, \frac{1}{2})$. Operator A corresponding to the strong formulation is defined as follows.

$$\begin{array}{ll} \mathbf{u} &= (\sigma, u) \\ \mathbf{H}^{-s}(\Omega) &= H^{-s}(\Omega)^2 \times H^{-s}(\Omega) \\ D(A) &:= H^{-s}(\operatorname{div}\Omega) \times H_0^{1-s}(\Omega) \subset \mathbf{H}^{-s}(\Omega) \\ A : & \mathbf{H}^{-s}(\Omega) \supset D(A) \to \mathbf{H}^{-s}(\Omega) \\ A\mathbf{u} &:= (\sigma - \nabla u, -\operatorname{div}\sigma) \end{array}$$

Its topological transpose is defined on the dual space,

$$\begin{array}{ll} \mathbf{v} &= (\tau,v) \\ \mathbf{H}^s(\Omega) &= H^s(\Omega)^2 \times H^s(\Omega) \\ D(A^*) &:= H^s(\operatorname{div}\Omega) \times H_0^{1+s}(\Omega) \subset \mathbf{H}^s(\Omega) \\ A^*: & \mathbf{H}^s(\Omega) \supset D(A^*) \to \mathbf{H}^s(\Omega) \\ A^*\mathbf{v} &:= (\tau + \nabla v, \operatorname{div}\sigma) \end{array}$$

Since we intend to pass with $s \to 0$, we assume a more regular than necessary load f = (0, f), $f \in L^2(\Omega)$. The UW formulation in the fractional spaces looks now as follows.

$$\begin{cases}
 u \in H^{-s}(\Omega) \\
 \langle u, A^* v \rangle = (f, v) \quad v \in D(A^*)
\end{cases}$$
(3.27)

where $\langle \cdot, \cdot \rangle$ denotes the duality pairing between $\mathsf{H}^{-s}(\Omega)$ and $\mathsf{H}^{s}(\Omega)$ and $D(A^*)$ is the subspace of the adjoint graph energy space,

$$\mathsf{H}_{A^*}(\Omega) := \left\{ \mathsf{v} \in \mathsf{H}^s(\Omega) \, : \, A^*\mathsf{v} \in \mathsf{H}^s(\Omega) \right\}.$$

THEOREM 1

The ultraweak variational formulation (3.27) is well-posed.

Proof:

Step 1: Operator A is bounded below. Let $I := (g, f) = Au = A(\sigma, u)$, i.e.,

$$\begin{aligned}
\sigma - \nabla u &= g \\
\operatorname{div} \sigma &= f.
\end{aligned} (3.28)$$

Testing the second equation with $v \in H_0^s(\operatorname{grad},\Omega) = H_0^{1+s}(\Omega)$, and integrating the left-hand side by parts, we obtain,

$$\langle \sigma, \nabla v \rangle = \langle f, v \rangle \quad v \in H^{1+s}_0(\Omega) \, .$$

Substituting $\sigma = \nabla u + g$, we get,

$$\langle \nabla u, \nabla v \rangle = \langle f, v \rangle - \langle g, \nabla v \rangle \quad v \in H_0^{1+s}(\Omega).$$

In other words, u satisfies the classical variational formulation discussed in the previous section. By the results obtained there, we have

$$||u||_{H^{1-s}(\Omega)} \le C||I||_{\mathsf{H}^{-s}(\Omega)}$$
.

But, simultaneously, from $(3.28)_1$,

$$\|\sigma\|_{H^{-s}(\Omega)} \le \|\nabla u\|_{H^{-s}(\Omega)} + \|g\|_{H^{-s}(\Omega)} \le C\|\mathbf{I}\|_{H^{-s}(\Omega)}$$

and, from $(3.28)_2$,

$$\|\operatorname{div}\sigma\|_{H^{-s}(\Omega)} \le \|f\|_{H^{-s}(\Omega)}$$

which shows that A is bounded below.

Step 2: Operator A^* is injective. Indeed, following a similar reasoning to the previous step, we first show that $\nabla v = 0$ in $H^s(\Omega)$ which implies that v is a constant. But the homogeneous BC on v implies that v must be zero. Consequently, $\tau = -\nabla v = 0$ as well.

Step 3: We invoke the Closed Range Theorem for Closed Operators that shows that A^* is bounded below with the same constant as operator A. Surjectivity and boundedness below of A^* implies now immediately that the bilinear form in the UW fomulation satisfies the inf-sup condition. Indeed, take any $u \in H^{-s}(\Omega)$. Let $w \in H^s(\Omega)$ be the Riesz representation of functional $\langle u, \cdot \rangle$. Take now the unique $v \in D(A^*)$ such that Av = w. We have,

$$\langle \mathsf{u}, A^* \mathsf{v} \rangle = \langle \mathsf{u}, \mathsf{w} \rangle = \|\mathsf{u}\|_{\mathsf{H}^{-s}(\Omega)}^2.$$

At the same time,

$$\|\mathbf{v}\|_{\mathbf{H}_{A^*}(\Omega)} \leq (1+\alpha^{-1})\|\mathbf{w}\|_{\mathbf{H}^s(\Omega)} = (1+\alpha^{-1})\|\mathbf{u}\|_{\mathbf{H}^{-s}(\Omega)}$$

where α is the boundedness below constant for operators A and A^* . Consequently,

$$\frac{\langle \mathsf{u}, A^* \mathsf{v} \rangle}{\|\mathsf{v}\|_{\mathsf{H}_{A^*}(\Omega)}} \geq (1 + \alpha^{-1})^{-1} \|\mathsf{u}\|_{\mathsf{H}^{-s}(\Omega)} \,.$$

The injectivity of A^* implies that space

$$V_0 := \{ \mathbf{v} \in D(A^*) : \langle \mathbf{u}, A^* \mathbf{v} \rangle = 0 \quad \forall \mathbf{u} \in \mathsf{H}^{-s}(\Omega) \}$$

is trivial and, therefore, the Babuška-Nečas Theorem implies that the UW variational formulation is well-posed.

Remark 3 One can follow the reasoning in [22] to show that the well-posedness of the UW formulation implies the well-posedness of the classical formulation. All three discussed formulations: the strong formulation, the classical one, and the UW formulation, are thus simultaneously well-posed.

4 Broken UW Variational Formulation

Equivalence of standard and localized fractional norms. Given a quasi-uniform, shape-regular FE mesh \mathcal{T}_h , we introduce the *localized fractional norm*,

$$||v||_{H^{\epsilon}(\mathcal{T}_h)}^2 := \sum_{K \in \mathcal{T}_h} ||v||_{H^{\epsilon}(K)}^2.$$
(4.29)

The localized norm is obviously bounded by the standard, global norm. The converse is also true, with an expected blow-up as $h \to 0$.

Lemma 2

There exists a constant C, independent of h such that

$$||v||_{H^{\epsilon}(\Omega)} \le Ch^{-\epsilon}||v||_{H^{\epsilon}(\mathcal{T}_h)} \quad v \in H^{\epsilon}(\Omega). \tag{4.30}$$

Proof: Let \mathcal{G} denote the family of pairs of neighboring elements (K_1, K_2) ,

$$\mathcal{G}:=\{(K_1,K_2)\in\mathcal{T}_h imes\mathcal{T}_h\,:\,ar{K}_1\capar{K}_2
eq\emptyset\}\quad G:=igcup_{(K_1,K_2)\in\mathcal{G}}K_1 imes K_2\,.$$

Consider the corresponding decomposition¹,

$$\Omega \times \Omega = G \cup G'$$
.

The assumption on shape regularity implies that the number of immediate neighbors for an element is uniformly bounded, i.e. the number of times each element K in the mesh appears as K_1 or K_2 in family \mathcal{G} , is bounded uniformly in K (with constant growing exponentially with dimension N). The assumption on quasi-uniformity implies that there exist constants c_1 , c_2 such that

$$c_1 h \leq h_K \leq c_2 h$$
 $K \in \mathcal{T}_h$.

This in turn implies that there exists a constant C > 0, such that

$$G' \subset \{(x,y) \in \Omega \times \Omega : |x-y| \ge Ch\}.$$

Consider now a pair $(K_1, K_2) \in \mathcal{G}$. We have,

$$\int_{K_1} \int_{K_2} \frac{|u(x) - u(y)|^2}{|x - y|^{N + 2\epsilon}} dx \, dy \le 2 \int_{K_1} \int_{K_2} \frac{|u(x)|^2}{|x - y|^{N + 2\epsilon}} dx \, dy + 2 \int_{K_1} \int_{K_2} \frac{|u(y)|^2}{|x - y|^{N + 2\epsilon}} dx \, dy.$$

¹Up to subsets of measure zero.

It is sufficient to focus on estimating one of the integrals only, say,

$$\int_{K_1} |u(x)|^2 \int_{K_2} \frac{1}{|x-y|^{N+2\epsilon}} dy \, dx \, .$$

Switching to spherical coordinates, we can estimate the inner integral,

$$\int_{K_2} \frac{1}{|x-y|^{N+2\epsilon}} dy \le |S_1| \int_{d(x,e)} \frac{1}{r^{N+2\epsilon}} r^{N-1} dr = \frac{|S_1|}{2\epsilon} d(x,e)^{-2\epsilon}$$

where $|S_1|$ is the measure of the unit sphere, and d(x, e) denotes the distance to a hypersurface e separating the two elements, see Fig. 4.1. We extend now u to a function $U \in C_0^{\infty}(\mathbb{R}^n)$. By Lemma 3.5.5 from [23],

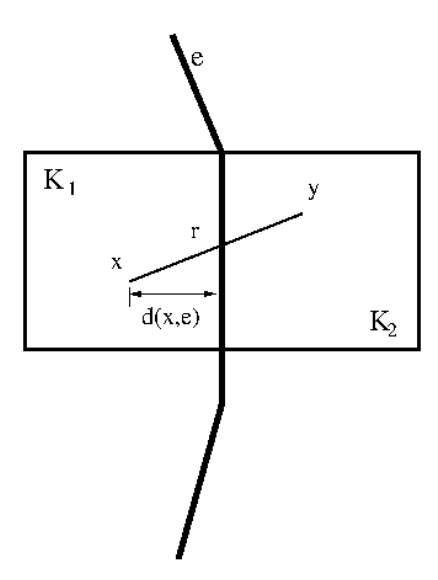


Figure 4.1: Estimation of double integral over two neighboring elements. Notation.

see also Remark 3.5.2 there, there exists a constant $C(\epsilon)$, $C(\epsilon) \to 1$ as $\epsilon \to 0$ such that

$$\int_{K_1} |u(x)|^2 d(x,e)^{-2\epsilon} dx \le C(\epsilon) \|U\|_{H^{\epsilon}(\mathbb{R}^n)}^2.$$

Passing to the minimum energy extension on the right-hand side, we obtain,

$$\int_{K_1} |u(x)|^2 d(x, e)^{-2\epsilon} dx \le C(\epsilon) ||u||_{H^{\epsilon}(K_1)}^2.$$

The integral over the complementary domain G' is estimated as follows.

$$\iint_{G'} \frac{|u(x) - u(y)|^2}{|x - y|^{N + 2\epsilon}} dxdy \leq 2 \iint_{G'} \frac{|u(x)|^2}{|x - y|^{N + 2\epsilon}} dxdy + 2 \iint_{G'} \frac{|u(y)|^2}{|x - y|^{N + 2\epsilon}} dxdy
= 4 \iint_{G'} \frac{|u(x)|^2}{|x - y|^{N + 2\epsilon}} dxdy.$$

The last integral is now estimated with the L^2 -norm,

$$\int_{\Omega} |u(x)|^2 \int_{|x-y| > h} \frac{1}{|x-y|^{N+2\epsilon}} \, dy \, dx \leq \int_{\Omega} |u(x)|^2 \int_{h}^{\infty} \frac{|S_1|}{r^{N+2\epsilon}} r^{N-1} \, dr \, dx$$
$$\leq \frac{|S_1|}{2\epsilon} h^{-2\epsilon} \int_{\Omega} |u(x)|^2 \, dx \, .$$

Remark 4 For polyhedral elements, the quasi-uniformity assumption on the mesh remains unaltered. However, the shape regularity needs to be understood differently. For the sake of Lemma 2, what matters is to have a uniform bound on the number of immediate neighbors an element can have. An effective way to bound such a quantity is to establish a maximum number of faces per polyhedral element. The higher such maximum is, the larger the equivalence constant may become.

Stability analysis for the broken UW variational formulation in fractional spaces. We reformulate now the UW formulation (1.2) in fractional spaces,

$$\begin{cases} \mathbf{u} \in \mathsf{H}^{-\epsilon}(\Omega), \ \hat{\mathbf{u}} := \widehat{(\sigma \cdot n}, \hat{u}) \in H^{-1/2 - \epsilon}(\Gamma_h) \times \widetilde{H}^{1/2 - \epsilon}(\Gamma_h) \\ \langle \mathbf{u}, A_h^* \mathbf{v} \rangle - \langle \hat{\mathbf{u}}, \mathbf{v} \rangle_{\Gamma_h} = (\mathsf{f}, \mathbf{v}) \quad \mathbf{v} \in V^{\epsilon}(\mathcal{T}_h) \,. \end{cases}$$
 (4.31)

Here $\langle \cdot, \cdot \rangle$ denotes the duality pairing between $\mathsf{H}^{-\epsilon}(\Omega)$ and $\mathsf{H}^{\epsilon}(\Omega)$, and

$$\begin{split} \mathsf{H}^{\pm\epsilon}(\Omega) &= H^{\pm\epsilon}(\Omega)^N \times H^{\pm\epsilon}(\Omega) \\ V^{\epsilon}(\mathcal{T}_h) &= H^{\epsilon}(\mathrm{div},\mathcal{T}_h) \times H^{\epsilon}(\mathrm{grad},\mathcal{T}_h) \\ H^{-1/2-\epsilon}(\Gamma_h) &= \{\hat{t} = \{t_K\}_{K \in \mathcal{T}_h} : \exists \, \sigma \in H^{-\epsilon}(\mathrm{div},\Omega) : t_K = \gamma_{n,\partial K} \sigma|_K \} \\ H^{1/2-\epsilon}(\Gamma_h) &= \{\hat{u} = \{u_K\}_{K \in \mathcal{T}_h} : \exists \, u \in H^{-\epsilon}(\mathrm{grad},\Omega) : u_K = \gamma_{\partial K} u|_K \} \end{split}$$

with

$$\langle \hat{\mathbf{u}}, \mathbf{v} \rangle_{\Gamma_h} = \sum_{K \in \mathcal{T}_h} \left[\langle \widehat{\sigma \cdot n}, v \rangle_{H^{-1/2 - \epsilon}(\partial K) \times H^{1/2 + \epsilon}(\partial K)} + \langle \hat{u}, \tau \cdot n \rangle_{H^{1/2 + \epsilon}(\partial K) \times H^{-1/2 - \epsilon}(\partial K)} \right] \,.$$

The trace spaces defined on the mesh skeleton are equipped with the minimum energy extension norms. The broken test spaces are equipped with the localized test norms derived from (4.29),

$$\begin{aligned} & \|\tau\|_{H^{\epsilon}(\mathrm{div},\mathcal{T}_h)}^2 &:= \sum_{K \in \mathcal{T}_h} \left[\|\tau\|_{H^{\epsilon}(K)}^2 + \|\mathrm{div}\,\tau\|_{H^{\epsilon}(K)}^2 \right] \\ & \|v\|_{H^{\epsilon}(\mathrm{grad},\mathcal{T}_h)}^2 &:= \sum_{K \in \mathcal{T}_h} \left[\|v\|_{H^{\epsilon}(K)}^2 + \|\mathrm{grad}\,\tau\|_{H^{\epsilon}(K)}^2 \right] \end{aligned}$$

Corollary 1 Let $v \in V^{\epsilon}(\mathcal{T}_h)$ be a broken test function. Lemma 2 implies that the union of A_h^*v is an element of $H^{\epsilon}(\Omega)$ and,

$$\begin{aligned} |\langle \mathbf{u}, A_h^* \mathbf{v} \rangle| &\leq C \|\mathbf{u}\|_{\mathsf{H}^{-\epsilon}(\Omega)} \|A_h^* \mathbf{v}\|_{\mathsf{H}^{\epsilon}(\Omega)} \leq C h^{-\epsilon} \|\mathbf{u}\|_{\mathsf{H}^{-\epsilon}(\Omega)} \|A_h^* \mathbf{v}\|_{\mathsf{H}^{\epsilon}(\mathcal{T}_h)} \\ &\leq C h^{-\epsilon} \|\mathbf{u}\|_{\mathsf{H}^{-\epsilon}(\Omega)} \|\mathbf{v}\|_{V^{\epsilon}(\mathcal{T}_h)}. \end{aligned} \tag{4.32}$$

The stability analysis follows closely the arguments from [12]. Let

$$\mathsf{I}(\mathsf{v}) := \langle \mathsf{u}, A_h^* \mathsf{v} \rangle - \langle \hat{\mathsf{u}}, \mathsf{v} \rangle_{\Gamma_h}$$
.

Stability of unbroken UW formulation implies the control of field variable u,

$$\begin{split} \gamma \|\mathbf{u}\|_{\mathsf{H}^{-\epsilon}(\Omega)} & \leq \sup_{\mathbf{v} \in V^{\epsilon}} \frac{|\langle \mathbf{u}, A_h^* \mathbf{v} \rangle|}{\|\mathbf{v}\|_{V^{\epsilon}}} \leq \sup_{\mathbf{v} \in V^{\epsilon}} \frac{|\langle \mathbf{u}, A_h^* \mathbf{v} \rangle|}{\|\mathbf{v}\|_{V^{\epsilon}(\mathcal{T}_h)}} = \sup_{\mathbf{v} \in V^{\epsilon}} \frac{|\langle \mathbf{u}, A_h^* \mathbf{v} \rangle - \langle \hat{\mathbf{u}}, \mathbf{v} \rangle_{\Gamma_h}|}{\|\mathbf{v}\|_{V^{\epsilon}(\mathcal{T}_h)}} \\ & \leq \sup_{\mathbf{v} \in V^{\epsilon}(\mathsf{T}_h)} \frac{|\mathsf{I}(\mathbf{v})|}{\|\mathbf{v}\|_{V^{\epsilon}(\mathcal{T}_h)}} =: \|\mathsf{I}\|_{(V^{\epsilon}(\mathcal{T}_h))'} \,. \end{split}$$

It follows that,

$$\sup_{\mathbf{v}\in V^{\epsilon}(\mathcal{T}_h)} \frac{|\langle \hat{\mathbf{u}}, \mathbf{v} \rangle_{\Gamma_h}|}{\|\mathbf{v}\|_{V^{\epsilon}(\mathcal{T}_h)}} \leq \|\mathbf{I}\|_{(V^{\epsilon}(\mathcal{T}_h))'} + Ch^{-\epsilon} \|\mathbf{u}\|_{\mathsf{H}^{-\epsilon}(\Omega)}$$
$$\leq (1 + C\gamma^{-1}h^{-\epsilon})\|\mathbf{I}\|_{(V^{\epsilon}(\mathcal{T}_h))'}.$$

As in [12], the big question is now whether the quantity on the left represents a norm and how to characterize it. Upon unpacking the duality pairing on the skeleton, we have,

$$\left(\sup_{\mathbf{v}\in V^{\epsilon}(\mathcal{T}_h)}\frac{|\langle\hat{\mathbf{u}},\mathbf{v}\rangle_{\Gamma_h}|}{\|\mathbf{v}\|_{V^{\epsilon}(\mathcal{T}_h)}}\right)^2 = \underbrace{\sum_{K\in\mathcal{T}_h}\left(\|\widehat{\boldsymbol{\sigma}\cdot\boldsymbol{n}}\|_{(H^{1/2+\epsilon}(\partial K))'}\right)^2}_{=:\|\widehat{\boldsymbol{\sigma}\cdot\boldsymbol{n}}\|_{H^{-1/2-\epsilon}(\Gamma_h)}^2} + \underbrace{\sum_{K\in\mathcal{T}_h}\left(\|\hat{\boldsymbol{u}}\|_{(H^{-1/2+\epsilon}(\partial K))'}\right)^2}_{=:\|\hat{\boldsymbol{u}}\|_{H^{1/2-\epsilon}(\Gamma_h)}^2} =:\|\hat{\boldsymbol{u}}\|^2$$

where the dual norms on the right-hand side are computed with respect to minimum energy extension norms.

$$\begin{aligned} \|\hat{v}\|_{H^{1/2+\epsilon}(\partial K)}^{2} &:= \inf_{\operatorname{tr}_{\partial K} v = \hat{v}} \left[\|v\|_{H^{\epsilon}(K)}^{2} + \|\operatorname{grad} v\|_{H^{\epsilon}(K)}^{2} \right] \\ \|\hat{t}\|_{H^{-1/2+\epsilon}(\partial K)}^{2} &:= \inf_{\operatorname{tr}_{n,\partial K} \tau = \hat{t}} \left[\|\tau\|_{H^{\epsilon}(K)}^{2} + \|\operatorname{div} \tau\|_{H^{\epsilon}(K)}^{2} \right] \end{aligned}$$
(4.33)

It has been shown in [23], Section 4.2, that the dual norms are equivalent to the minimum energy extension norms,

$$\|\widehat{\sigma \cdot n}\|_{H^{-1/2-\epsilon}(\partial K)}$$
 and $\|\hat{u}\|_{H^{1/2-\epsilon}(\partial K)}$.

This implies that the supremum represents indeed a norm. Control of equivalence constants is more delicate. The dual norms are bounded with minimum energy extension norm (with a unit equivalence constant). This will help with the estimation of the best approximation error. However, the estimation of the equivalence constant in the other direction involves a partition of unity argument which makes, a priori, the constant dependent upon the domain (in our case, an element K). Note that, for $\epsilon = 0$, the dual and minimum energy extension norms are equal [12, 23].

We summarize our findings in the following theorem.

THEOREM 2

The following inf-sup condition holds:

$$\min(\gamma, (1 + C\gamma^{-1}h^{\epsilon})^{-1}) \left(\|\mathbf{u}\|_{\mathsf{H}^{-\epsilon}(\Omega)}^2 + \|\hat{\mathbf{u}}\|^2 \right)^{\frac{1}{2}} \le \|\mathsf{I}\|_{(V^{\epsilon}(\mathcal{T}_h))'} = \sup_{\mathbf{v} \in V^{\epsilon}(\mathcal{T}_h)} \frac{|\langle \mathbf{u}, A_h \mathbf{v} \rangle + \langle \hat{\mathbf{u}}, \mathbf{v} \rangle_{\Gamma_h}|}{\|\mathbf{v}\|_{V^{\epsilon}(\mathcal{T}_h)}}$$
(4.34)

More precisely,

$$\gamma \|\mathbf{u}\| \le \|\mathbf{I}\|_{(V^{\epsilon}(\mathcal{T}_h))'}$$
$$(C\gamma^{-1}h^{-\epsilon})^{-1}\|\hat{\mathbf{u}}\| \le \|\mathbf{I}\|_{(V^{\epsilon}(\mathcal{T}_h))'}$$

THEOREM 3

Let (u_h, \hat{u}_h) be the ideal DPG method solution where $\hat{u}_h = (\widehat{\sigma \cdot n_h}, \hat{u}_h)$. The following a-priori error estimates hold:

$$\gamma \|\mathbf{u} - \mathbf{u}_{h}\|_{\mathsf{H}^{-\epsilon}(\Omega)} \leq Ch^{-\epsilon} \inf_{\mathsf{w}_{h}} \|\mathbf{u} - \mathsf{w}_{h}\|_{\mathsf{H}^{-\epsilon}(\Omega)} \\
+ \left(\sum_{K \in \mathcal{T}_{h}} \{ \inf_{\hat{t}_{h}} \|\sigma \cdot n - \hat{t}_{h}\|_{H^{-1/2 - \epsilon}(\partial K)}^{2} + \inf_{\hat{w}_{h}} \|u - \hat{w}_{h}\|_{H^{1/2 - \epsilon}(\partial K)}^{2} \} \right)^{\frac{1}{2}}$$
(4.35)

and

$$(1 + C\gamma^{-1}h^{-\epsilon})^{-1} \quad \left(\sum_{K \in \mathcal{T}_{h}} \{\|\sigma \cdot n - \widehat{\sigma \cdot n_{h}}\|_{(H^{1/2 + \epsilon}(\partial K))'}^{2} + \|u - \hat{u}_{h}\|_{(H^{-1/2 + \epsilon}(\partial K))'}^{2}\}\right)^{\frac{1}{2}} \\ \leq Ch^{-\epsilon} \inf_{\mathbf{w}_{h}} \|\mathbf{u} - \mathbf{w}_{h}\|_{\mathbf{H}^{-\epsilon}(\Omega)} \\ + \left(\sum_{K \in \mathcal{T}_{h}} \{\inf_{\hat{t}_{h}} \|\sigma \cdot n - \hat{t}_{h}\|_{H^{-1/2 - \epsilon}(\partial K)}^{2} + \inf_{\hat{w}_{h}} \|u - \hat{w}_{h}\|_{H^{1/2 - \epsilon}(\partial K)}^{2}\}\right)^{\frac{1}{2}}.$$

$$(4.36)$$

Proof: We only need to recall continuity estimate (4.32) and use the bound:

$$|\sum_{K\in\mathcal{T}_h}(\langle\widehat{\sigma\cdot n},v\rangle_{\partial K}+\langle\widehat{u},\tau\cdot n\rangle_{\partial K})|\leq (\sum_{K\in\mathcal{T}_h}(\|\widehat{\sigma\cdot n}\|_{H^{-1/2-\epsilon}(\partial K)}^2+\|\widehat{u}\|_{H^{1/2-\epsilon}(\partial K)}^2))^{\frac{1}{2}}\,\|\mathbf{v}\|_{V^{\epsilon}(\mathcal{T}_h)}\,.$$

5 Implications for the Non-conforming DPG Method

In the preceding sections we have developed a theory for a DPG method formulated in fractional spaces. By weakening the trial norm and strengthening the test norm, we have been able to employ the discontinuous discretization of traces which, in the relaxed energy setting, has become conforming. The discussed results

require computations with the stronger, fractional test norm which is not attractive at all from the practical point of view.

In this section, we show how one can combine arguments developed in [36] to conclude semioptimal convergence results in the weaker, fractional $H^{-\epsilon}$ norms, computing with the standard test norm. In other words, we change the analysis but not the computations.

We begin by recalling the results from [36] formulated in an abstract form. We assume that we can introduce an alternate functional setting with a stronger test norm $||v||_{\mathcal{V}}$, and a weaker trial norm $||u||_{\mathcal{U}}$,

$$||v||_V \le ||v||_{\mathcal{V}} \quad v \in \mathcal{V} \subset V \quad \text{and} \quad ||u||_{\mathcal{U}} \le ||u||_U \quad u \in U \subset \mathcal{U}.$$

We postulate now that the following conditions are satisfied.

Assumption 1: Inf-sup condition in the modified setting,

$$\widetilde{\gamma} \|u\|_{\mathcal{U}} \le \sup_{v \in \mathcal{V}} \frac{|b(u, v)|}{\|v\|_{\mathcal{V}}}.$$

Assumption 2: Existence of Fortin operators for the *stronger* test norm, leading to the discrete stability in the weaker norm,

$$\frac{\widetilde{\gamma}}{C_F} \|u_h\|_{\mathcal{U}} \leq \sup_{v_h \in V_r} \frac{|b(u_h, v_h)|}{\|v_h\|_{\mathcal{V}}} \leq \sup_{v_h \in V_r} \frac{|b(u_h, v_h)|}{\|v_h\|_{\mathcal{V}}} \quad u_h \in U_h \subset \mathcal{U}.$$

Assumption 3: Continuity of the bilinear form on the finite-dimensional enriched test space,

$$|b(u, v_h)| \le M_r ||u||_{\mathcal{U}} ||v_h||_V \quad v_h \in V_r \subset \mathcal{V}.$$

Assumption 4: Galerkin orthogonality,

$$b(u_h - u, v) = 0$$
 $u \in \mathcal{U}, u_h \in U_h \subset \mathcal{U}, v \in \mathbf{T}^r(U_h)$

where $\mathbf{T}^r:U\to V_r$ is the approximate trial-to-test operator corresponding to the original test norm.

With the four assumptions satisfied, we can use now the standard Strang's argument to establish the following a-priori estimate in the weaker norm.

$$\begin{split} \|u-u_h\|_{\mathcal{U}} & \leq \|u-w_h\|_{\mathcal{U}} + \|w_h-u_h\|_{\mathcal{U}} & \text{(triangle inequality)} \\ & \leq \|u-w_h\|_{\mathcal{U}} + \frac{C_F}{\widetilde{\gamma}} \sup_{v_h \in V_r} \frac{|b(w_h-u_h,v_h)|}{\|v_h\|_V} & \text{(discrete stability)} \\ & = \|u-w_h\|_{\mathcal{U}} + \frac{C_F}{\widetilde{\gamma}} \sup_{v_h \in T^r(U_h)} \frac{|b(w_h-u_h,v_h)|}{\|v_h\|_V} & \text{(definition of optimal test functions)} \\ & = \|u-w_h\|_{\mathcal{U}} + \frac{C_F}{\widetilde{\gamma}} \sup_{v_h \in T^r(U_h)} \frac{|b(w_h-u,v_h)|}{\|v_h\|_V} & \text{(Galerkin orthogonality)} \\ & \leq (1 + \frac{C_F}{\widetilde{\gamma}} M_r) \|u-w_h\|_{\mathcal{U}}. \end{split}$$

We now verify the assumptions.

- The inf-sup condition for the fractional setting has been proved in Theorem 2. Inf-sup constant $\tilde{\gamma}$ is of order h^{ϵ} . For the fields alone, the inf-sup constant is of order one.
- Construction of the Fortin operators has been delegated to Appendix A. For tetrahedral meshes, we are able to employ any of the existing H^1 Fortin operators and, following [36], the standard Raviart-Thomas interpolation operator for the H(div) Fortin operator. Moreover, the construction extends to arbitrary polyhedral meshes, provided we use tetrahedral subelement meshes to define the enriched spaces. Due the scaling properties of the fractional norm, the Fortin constant is of order $h^{-\epsilon}$.
- The continuity of the bilinear form for enriched space test functions is based on the finite-dimensionality argument. For instance,

$$\begin{split} \|\tau\|_{H^{\epsilon}(T)}^2 & \lesssim h^{-1-2\epsilon} \|\hat{\tau}\|_{H^{\epsilon}(\hat{T})}^2 & \text{(scaling for Piola transform)} \\ & \lesssim C(r)h^{-1-2\epsilon} \|\hat{\tau}\|_{L^2(\hat{T})}^2 & \text{(finite dimensionality argument)} \\ & \lesssim C(r)h^{-2\epsilon} \|\tau\|_{L^2(T)}^2 & \text{(scaling for Piola transform)} \,. \end{split}$$

The norm equivalence constant clearly depends upon the order r of the enriched space, but for limited range of ϵ , it can be claimed to be independent of ϵ . In the end, the continuity constant is $M_r \approx$ $C(r)h^{-2\epsilon}$. One factor h^{ϵ} is lost due to the scaling properties discussed above, the other comes from the global continuity estimate (4.32).

• The Galerkin orthogonality condition is clearly satisfied.

THEOREM 4

Let (u_h, \hat{u}_h) be the practical DPG method solution where $\hat{u}_h = (\widehat{\sigma \cdot n_h}, \hat{u}_h)$. The following a-priori error estimates hold.

$$\|\mathbf{u} - \mathbf{u}_h\|_{\mathsf{H}^{-\epsilon}(\Omega)} \le$$

$$C(\epsilon)h^{-3\epsilon} \left\{ \inf_{\mathsf{w}_{h}} \|\mathsf{u} - \mathsf{w}_{h}\|_{\mathsf{H}^{-\epsilon}(\Omega)} + \left(\sum_{K \in \mathcal{T}_{h}} \left[\inf_{\hat{t}_{h}} \|\sigma \cdot n - \hat{t}_{h}\|_{H^{-1/2 - \epsilon}(\partial K)}^{2} + \inf_{\hat{w}_{h}} \|u - \hat{w}_{h}\|_{H^{1/2 - \epsilon}(\partial K)}^{2} \right] \right)^{\frac{1}{2}} \right\}$$
(5.37)

and

$$(\sum_{K \in \mathcal{T}_{h}} \{ \| \sigma \cdot n - \widehat{\sigma \cdot n_{h}} \|_{(H^{1/2 + \epsilon}(\partial K))'}^{2} + \| u - \hat{u}_{h} \|_{(H^{-1/2 + \epsilon}(\partial K))'}^{2} \})^{\frac{1}{2}}$$

$$\leq C(\epsilon) h^{-4\epsilon} \left\{ \inf_{\mathsf{w}_{h}} \| \mathsf{u} - \mathsf{w}_{h} \|_{\mathsf{H}^{-\epsilon}(\Omega)} + (\sum_{K \in \mathcal{T}_{h}} [\inf_{\hat{t}_{h}} \| \sigma \cdot n - \hat{t}_{h} \|_{H^{-1/2 - \epsilon}(\partial K)}^{2} + \inf_{\hat{w}_{h}} \| u - \hat{w}_{h} \|_{H^{1/2 - \epsilon}(\partial K)}^{2}])^{\frac{1}{2}} \right\}.$$

$$(5.38)$$

Above, $\epsilon \in (0, \frac{1}{2})$ and stability constant $C(\epsilon) \to \infty$ as $\epsilon \to 0$.

6 Best Approximation Error Estimates for Polyhedral Elements

6.1 Best Approximation Error Estimate for the Minimum Energy Extension $H^{1/2-\epsilon}$ Norm

The philosophy of developing the best approximation error estimates mirrors the classical approach for finite elements. We move to a master element, apply the Bramble-Hilbert argument, and pullback to the physical element with the proper power of element size resulting from scaling the Sobolev seminorms. There are several delicate steps in the derivations presented next. First of all, all norms equivalence arguments are to be executed only on the master element. In this way, we employ a number of constants that depend upon the master element but not a particular physical element. Secondly, contrary to standard meshes with affine elements, we are dealing not with a single master element but rather a family of "unit" finite elements of different shape and number of faces. Hence we have to make perhaps a "hand-waving" assumption that the constants are uniformly bounded for all our "master elements".

Given an element K, we begin with the estimation of the norm dual to the minimum energy extension norm $\|\tau \cdot n\|_{H^{-1/2+\epsilon}(\partial K)}$,

$$||u||_{(H^{-1/2+\epsilon}(\partial K))'} = \sup_{\tau \in H^{\epsilon}(\operatorname{div},K)} \frac{|\langle u, \tau \cdot n \rangle_{\partial K}|}{||\tau||_{H^{\epsilon}(\operatorname{div},K)}}.$$

Let $u \in H^{1/2-\epsilon}(\partial K)$ and let $U \in H^{\epsilon}(\operatorname{grad},K)$ be an arbitrary lift of u. We have,

$$(*) := \left(\sup_{\tau \in H^{\epsilon}(\operatorname{div},K)} \frac{|\langle u, \tau \cdot n \rangle_{\partial K}|}{\|\tau\|_{H^{\epsilon}(\operatorname{div},K)}}\right)^{2} = \left(\sup_{\tau \in H^{\epsilon}(\operatorname{div},K)} \frac{|\langle U, \operatorname{div}\tau \rangle + \langle \nabla U, \tau \rangle|}{(\|\tau\|_{H^{\epsilon}(K)}^{2} + \|\operatorname{div}\tau\|_{H^{\epsilon}(K)}^{2})^{1/2}}\right)^{2}$$

$$= \left(\sup_{\hat{\tau} \in H^{\epsilon}(\widehat{\operatorname{div}},\hat{K})} \frac{|\langle \hat{U}, \widehat{\operatorname{div}}\hat{\tau} \rangle + \langle \hat{\nabla}\hat{U}, \hat{\tau} \rangle|}{(h^{-1}\|\hat{\tau}\|_{L^{2}(\hat{K})}^{2} + h^{-1+2\epsilon}|\hat{\tau}|_{H^{\epsilon}(\hat{K})}^{2} + h^{-3}\|\widehat{\operatorname{div}}\hat{\tau}\|_{L^{2}(\hat{K})}^{2} + h^{-3+2\epsilon}\|\widehat{\operatorname{div}}\hat{\tau}\|_{H^{\epsilon}(\hat{K})}^{2}}\right)^{2}$$

$$\leq \left(\sup_{\hat{\tau} \in H^{\epsilon}(\widehat{\operatorname{div}},\hat{K})} \frac{|\langle \hat{U}, \widehat{\operatorname{div}}\hat{\tau} \rangle + \langle \hat{\nabla}\hat{U}, \hat{\tau} \rangle|}{(h^{-1+2\epsilon}\|\hat{\tau}\|_{H^{\epsilon}(\hat{K})}^{2} + h^{-3+2\epsilon}\|\widehat{\operatorname{div}}\hat{\tau}\|_{H^{\epsilon}(\hat{K})}^{2}}\right)^{1/2} \right)^{2}$$

Above, element \hat{K} is a unit element (with $h_{\hat{K}}=1$) obtained by translation and simple scaling of element K of size h. We employ the standard Piola transforms for the exact sequence elements,

$$U = \hat{U}, \quad E = h^{-1}\hat{E}, \quad \tau = h^{-2}\hat{\tau}, \quad f = h^{-3}\hat{f}.$$

Note that $(U,f)_K=(\hat{U},\hat{f})_{\hat{K}}$ and $(E,\tau)_K=(\hat{E},\hat{\tau})_{\hat{K}}$ for (regular) functions. The scaling extends to duality pairing by a density argument or, equivalently, by using it as a definition of transform for elements $U\in H^{-\epsilon}(\operatorname{grad},K)$ and $E\in H^{-\epsilon}(\operatorname{curl},K)$.

We follow with the estimation,

$$(*) \le h^{3-2\epsilon} \|\hat{U}\|_{H^{-\epsilon}(\hat{K})}^2 + h^{1-2\epsilon} \|\hat{\nabla}\hat{U}\|_{H^{-\epsilon}(\hat{K})}^2 \le h^{1-2\epsilon} \|\hat{U}\|_{H^{-\epsilon}(\operatorname{grad},\hat{K})}^2$$

Consequently, the original dual norm is estimated with the minimum energy extension norm of \hat{u} ,

$$(*) \le h^{1-2\epsilon} \|\hat{u}\|_{H^{1/2-\epsilon}(\partial \hat{K})}^2.$$

We employ now the localization argument,

$$h^{1-2\epsilon} \|\hat{u}\|_{H^{1/2-\epsilon}(\partial \hat{K})}^2 \le C(\epsilon) \sum_{\hat{f} \subset \partial \hat{K}} \|\hat{u}\|_{H^{1/2-\epsilon}(\hat{f})}^2$$

where the summation extends over all faces \hat{f} of the unit element. Constant $C(\epsilon)$ blows up at rate ϵ^{-1} (see [25]), and it does depend upon the topology and shape of the unit element.

We define now the approximation $u_p \in \mathcal{P}^p(f)$ in such a way that $\hat{u}_p \in \mathcal{P}^p(\hat{f})$ is the orthogonal projection of \hat{u} onto the polynomial space in the $H^{1/2-\epsilon}$ -norm,

$$\hat{u}_p := \arg\min_{\hat{w}_p \in \mathcal{P}(\hat{f})} \|\hat{u} - \hat{w}_p\|_{H^{1/2 - \epsilon}(\hat{f})}.$$

Employing the Bramble-Hilbert argument, we get,

$$\left(\sup_{\tau \in H^{\epsilon}(\operatorname{div},K)} \frac{|\langle u - u_p, \tau \cdot n \rangle_{\partial K}|}{\|\tau\|_{H^{\epsilon}(\operatorname{div},K)}}\right)^{2} \leq C(\epsilon)h^{1-2\epsilon} \sum_{\hat{f}} \inf_{\hat{w}_{p}} \|\hat{u} - \hat{w}_{p}\|_{H^{1/2-\epsilon}(\hat{f})}^{2}
\leq C(\epsilon)h^{1-2\epsilon} \sum_{\hat{f}} \inf_{\hat{w}_{p}} \|\hat{u} - \hat{w}_{p}\|_{H^{r}(\hat{f})}^{2}
\leq C(r)C(\epsilon)h^{1-2\epsilon} \sum_{\hat{f}} |\hat{u}|_{H^{r}(\hat{f})}^{2}
\leq C(r)C(\epsilon)h^{2r-1-2\epsilon} \sum_{f} |u|_{H^{r}(f)}^{2}$$

for any $r \leq p+1$. C(r) is the Bramble-Hilbert constant or, more precisely, the maximum constant for all the involved faces. For the maximum r=p+1 this leads to the expected rate of convergence,

$$\sup_{\tau \in H^{\epsilon}(\operatorname{div},K)} \frac{|\langle u - u_p, \tau \cdot n \rangle_{\partial K}|}{\|\tau\|_{H^{\epsilon}(\operatorname{div},K)}} \le C(r)C(\epsilon)h^{p + \frac{1}{2} - \epsilon} \left(\sum_{f} |u|_{H^{p+1}(f)}^2\right)^{1/2} \tag{6.39}$$

If we limit ourselves to less regular functions $u \in H^{p+\frac{1}{2}}(f)$, by using a (non-trivial) interpolation argument we obtain the expected $h^{p-\epsilon}$ rate of convergence.

For different elements K, we obtain the corresponding, different unit "master" elements \hat{K} . In order to make the derived estimate useful, we have to assume that the class of the unit elements we obtain, is either finite or that the corresponding localization constant $C(\epsilon)$ and Bramble-Hilbert constant C(r) are uniformly bounded in \hat{K} .

6.2 Best Approximation Error Estimate for the Minimum Energy Extension $H^{-1/2}$ Norm

This time we use a different idea. We introduce a polyhedral $H(\operatorname{div})$ -conforming FE element with an "infinite number of bubbles" and develop an interpolation error estimate for such an element. Let $L^2_{\operatorname{avg}}(K)$ denote the subspace of $L^2(K)$ functions with zero average,

$$L^2_{\text{avg}}(K) := \{ q \in L^2(K) : \int_K q = 0 \}.$$

Lemma 3

Let K be an arbitrary polyhedron with flat faces f.

- 1. For every $q \in L^2_{avg}(K)$, there exists a bubble $\sigma \in H_0(\text{div}, K)$ such that $\text{div}\sigma = q$.
- 2. For every face f, and an arbitrary $t \in \mathcal{P}(f)$, there exists a function $\sigma \in H(\text{div}, K)$ such that normal trace $\sigma \cdot n = t$ on the face f, and it vanishes on the remaining faces.

-

Proof:

1. Consider the Neumann problem,

$$\begin{cases} U \in H^1(K) \\ \int_K \nabla U \cdot \nabla V = \int_K q V \quad V \in H^1(K) \end{cases}$$

and take $\sigma = -\nabla U$.

2. Consider the Neumann problem,

$$\left\{ \begin{array}{l} U \in H^1(K) \\ \int_K \nabla U \cdot \nabla V + U \, V = \int_f t \, V \quad V \in H^1(K) \end{array} \right.$$

and take $\sigma = -\nabla U$. Note that $\mathrm{div}\sigma = -\Delta U = -U \in L^2(K)$.



We introduce now a "finite element" with the FE space defined as

$$V^{p}(K) := \{ \sigma \in H(\text{div}, K) : \sigma \cdot n \in \mathcal{P}^{p}(f), \text{ for every face } f \subset \partial K \}.$$
 (6.40)

and the corresponding Projection-Based (PB) Interpolant [29] $\sigma_p \in V^p(K), \sigma_p = \Pi \sigma$ defined as follows.

$$\begin{cases} \|\sigma_p \cdot n - \sigma \cdot n\|_{L^2(f)} \to \min & \text{for every face } f \subset \partial K \\ \|\operatorname{div}(\sigma_p - \sigma)\|_{L^2(K)} \to \min & \\ (\sigma - \sigma_p, \nabla \times F)_K = 0 & F \in H_0(\operatorname{curl}, K) \end{cases}$$
(6.41)

for sufficiently regular functions σ . By Lemma 3, the FE space is well defined, and $\operatorname{div} \sigma_p = \operatorname{div} \sigma$. Indeed, condition (6.41)₂ implies that

$$(\operatorname{div}(\sigma_p - \sigma), q) = 0$$
 for every $q \in L^2_{avg}(K)$.

At the same time, condition $(6.41)_1$ implies that

$$\int_{K} \operatorname{div}(\sigma_{p} - \sigma) = \int_{\partial K} (\sigma_{p} - \sigma) \cdot n = 0.$$

The $H(\operatorname{div})$ -norm of the interpolation error reduces thus just to the L^2 -norm. Let $\sigma \in H(\operatorname{div}, K)$ be now a sufficiently regular function defined on a polyhedral element K. As usual, we pullback σ to the master element \hat{K} , determine the PB interpolant $\hat{\sigma}$ there and push it forward to element K. We proceed with the standard derivation of the interpolation error.

$$\begin{split} \|\sigma - \sigma_p\|_{L^2(K)} &= h^{-1/2} \|\hat{\sigma} - \hat{\sigma}_p\|_{L^2(\hat{K})} \\ &= h^{-1/2} \|(\hat{I} - \hat{\Pi})\hat{\sigma}\|_{L^2(\hat{K})} \\ &= h^{-1/2} \|(\hat{I} - \hat{\Pi})(\hat{\sigma} - \hat{\tau}_p)\|_{L^2(\hat{K})} \\ &= h^{-1/2} \|(\hat{I} - \hat{\Pi})(\hat{\sigma} - \hat{\tau}_p)\|_{L^2(\hat{K})} \\ &\leq h^{-1/2} \|\hat{I} - \hat{\Pi}\|_{\mathcal{L}(H^r(\hat{K}), L^2(\hat{K}))} \|\hat{\sigma} - \hat{\tau}_p\|_{H^r(\hat{K})} \end{split}$$
 (polynomial preservation property)

for any polynomial $\hat{\tau}_p \in (\mathcal{P}^{p-1}(\hat{K})^3$, and $r \leq p$. We finish by applying the Bramble-Hilbert and scaling arguments,

$$\|\sigma - \sigma_p\|_{L^2(K)} \le Ch^{-1/2} \inf_{\hat{\tau} \in \mathcal{P}^{p-1}(\hat{K})} \|\hat{\sigma} - \hat{\tau}_p\|_{H^r(\hat{K})} \le Ch^{-1/2} |\hat{\sigma}|_{H^r(\hat{K})} \le Ch^r |\sigma|_{H^r(K)}.$$

For r=p we obtain the expected p-rate of convergence in presence of no limitations coming from the regularity of the solution.

The H(div)-interpolation result leads immediately to the best approximation error estimate in the minimum energy extension norm $H^{-1/2}(\partial K)$,

$$\inf_{t_p \in \mathcal{P}_d^p(\partial K)} \|\sigma \cdot n - t_p\|_{H^{-1/2}(\partial K)} \le \|\sigma - \Pi\sigma\|_{H(\operatorname{div},K)} \le Ch^p |\sigma|_{H^p(K)}. \tag{6.42}$$

6.3 L^2 Projection Error Estimate

The standard scaling and Bramble-Hilbert arguments lead to the estimate,

$$\inf_{v_p \in \mathcal{P}^{p-1}(K)} \|u - v_p\|_{L^2(K)} \le Ch^p |u|_{H^p(K)}. \tag{6.43}$$

7 A Priori Error Estimates

7.1 A Priori Error Estimates for the Ideal Fractional DPG Method

Polyhedra with triangular or quadrilateral faces. We recall first the standard way to approximate the best approximation error for traces in the minimum energy extension norms under the assumption that trace \hat{u} is discretized with trace \hat{w}_h of standard, H^1 -conforming finite element function w_h . We have for the $H^{1/2}$ -traces,

$$\begin{split} \inf_{\hat{w}_h} \|u - \hat{w_h}\|_{H^{1/2}(\partial K)} & \leq \|u - w_h\|_{H^1(K)} & \text{(definition of minimum energy extension norm)} \\ & \leq \|u - \Pi_h^{\text{grad}} u\|_{H^1(K)} \\ & \leq C h^p \|u\|_{H^{p+1}(K)} \;, \end{split}$$

with C independent of element K and function u.

A similar argument holds for the $H^{-1/2}$ normal trace,

$$\begin{split} \inf_{\hat{t}_h} \|\sigma \cdot n - \hat{t_h}\|_{H^{-1/2}(\partial K)} & \leq \|\sigma - v_h\|_{H(\operatorname{div},K)} & \text{ (definition of minimum energy extension norm)} \\ & \leq \|\sigma - \Pi_h^{\operatorname{div}}\sigma\|_{H(\operatorname{div},K)} \\ & \leq Ch^p \|\sigma\|_{H^p(\operatorname{div},K)} \\ & \leq Ch^p \|u\|_{H^{p+1}(K)} \,. \end{split}$$

The argument extends easily from a standard element to a polyhedron with triangular or quadrilateral faces under the assumption that the polyhedron can be meshed with a submesh consisting of standard *shape regular* subelements.

Stability estimates (4.35) and (4.36) lead directly to the a-priori error estimates for the ideal DPG method:

$$\begin{aligned}
&\{\gamma \| \mathbf{u} - \mathbf{u}_{h} \|_{\mathsf{H}^{-\epsilon}(\Omega)}, (1 + C\gamma^{-1}h^{-\epsilon})^{-1} \left(\sum_{K \in \mathcal{T}_{h}} \{ \| \sigma \cdot n - \widehat{\sigma \cdot n}_{h} \|_{(H^{1/2 - \epsilon}(\partial K))'}^{2} + \| u - \widehat{u}_{h} \|_{(H^{-1/2 - \epsilon}(\partial K))'}^{2} \right)^{\frac{1}{2}} \} \\
&\leq Ch^{-\epsilon} \inf_{\mathbf{w}_{h}} \| \mathbf{u} - \mathbf{w}_{h} \|_{\mathsf{H}^{-\epsilon}(\Omega)} + \left(\sum_{K \in \mathcal{T}_{h}} \{ \inf_{\widehat{t}_{h}} \| \sigma \cdot n - \widehat{t}_{h} \|_{H^{-1/2 - \epsilon}(\partial K)}^{2} + \inf_{\widehat{w}_{h}} \| u - \widehat{w}_{h} \|_{H^{1/2 - \epsilon}(\partial K)}^{2} \right)^{\frac{1}{2}} \\
&\leq Ch^{p - \epsilon} \| u \|_{H^{p + 1}(\Omega)}
\end{aligned} \tag{7.44}$$

with constants C independent of ϵ .

Polyhedra with general polygonal faces. As above, we estimate the $H^{-\epsilon}$ error with the L^2 -error, and the minimum energy extension $H^{-1/2-\epsilon}$ error with the minimum energy extension $H^{-1/2}$ error. The best approximation error estimates (6.39), (6.42), and (6.43) lead to the final estimate:

$$\begin{aligned}
&\{\gamma \| \mathbf{u} - \mathbf{u}_{h} \|_{\mathsf{H}^{-\epsilon}(\Omega)}, (1 + C\gamma^{-1}h^{-\epsilon})^{-1} \left(\sum_{K \in \mathcal{T}_{h}} \{ \| \sigma \cdot n - \widehat{\sigma \cdot n}_{h} \|_{(H^{1/2 - \epsilon}(\partial K))'}^{2} + \| u - \widehat{u}_{h} \|_{(H^{-1/2 - \epsilon}(\partial K))'}^{2} \right)^{\frac{1}{2}} \} \\
&\leq Ch^{-\epsilon} \inf_{\mathsf{w}_{h}} \| \mathbf{u} - \mathsf{w}_{h} \|_{\mathsf{H}^{-\epsilon}(\Omega)} + \left(\sum_{K \in \mathcal{T}_{h}} \{ \inf_{\widehat{t}_{h}} \| \sigma \cdot n - \widehat{t}_{h} \|_{H^{-1/2 - \epsilon}(\partial K)}^{2} + \inf_{\widehat{w}_{h}} \| u - \widehat{w}_{h} \|_{H^{1/2 - \epsilon}(\partial K)}^{2} \right)^{\frac{1}{2}} \\
&\leq Ch^{p - \epsilon} \| u \|_{H^{p + 1}(\Omega)} + C(\epsilon)h^{p + \frac{1}{2} - \epsilon} \left(\sum_{f} \| u \|_{H^{p + 1}(f)}^{2} \right)^{\frac{1}{2}}
\end{aligned} \tag{7.45}$$

The best approximation error estimate includes a blow up constant $C(\epsilon)$ but, in presence of regular solution, the extra compensating 1/2 convergence rate factor as well.

7.2 A Priori Error Estimates for the Practical Non-conforming DPG Method in Fractional Norms

We restrict ourselves to the polyhedral meshes only. Theorem 4 and the best approximation error estimates (6.39), (6.42), and (6.43) lead to the final estimates:

$$\|\mathbf{u} - \mathbf{u}_{h}\|_{\mathbf{H}^{-\epsilon}(\Omega)} \leq C(\epsilon)h^{-3\epsilon} \left\{ Ch^{p-\epsilon} \|u\|_{H^{p+1}(\Omega)} + C(\epsilon)h^{p+\frac{1}{2}-\epsilon} \left(\sum_{f} \|u\|_{H^{p+1}(f)}^{2} \right)^{\frac{1}{2}} \right\}$$

$$\left(\sum_{K \in \mathcal{T}_{h}} \{ \|\sigma \cdot n - \widehat{\sigma \cdot n}_{h}\|_{(H^{1/2+\epsilon}(\partial K))'}^{2} + \|u - \widehat{u}_{h}\|_{(H^{-1/2+\epsilon}(\partial K))'}^{2} \} \right)^{\frac{1}{2}}$$

$$\leq C(\epsilon)h^{-4\epsilon} \left\{ Ch^{p-\epsilon} \|u\|_{H^{p+1}(\Omega)} + C(\epsilon)h^{p+\frac{1}{2}-\epsilon} \left(\sum_{f} \|u\|_{H^{p+1}(f)}^{2} \right)^{\frac{1}{2}} \right\} .$$

$$(7.46)$$

There are two blow up constants above, both denoted with the same symbol $C(\epsilon)$. The first one comes form the construction of the Fortin operator which is invalid in the limit $\epsilon=0$, the second one from the localization argument in the best approximation minimum energy extension $H^{1/2-\epsilon}$ error estimate.

8 Numerical Experiments

8.1 About the implementation

A modified version of the hp-adaptive finite element code hp3D by Demkowicz et al. (see [28]) has been implemented in order to support high-order approximation with (simple) polyhedral elements of arbitrary number of vertices and (flat) faces. The new code is able to obtain the practical DPG solution of any well-posed broken ultraweak variational formulation, but with discontinuous discrete traces. However, when all faces in the mesh skeleton are triangular, the code can enforce continuity of the traces if wanted.

This PolyDPG code uses the polynomial spaces for tetrahedra for the element variables, and those of the triangle for the face variables. Integration of the local Gram and stiffness matrices is carried out using the so called *homogeneous numerical integration (HNI)*, which needs homogeneous integrands to transform volume integrals into boundary integrals for any convex or non-convex polyhedron [39, 42, 16]. To take advantage of this technique, the bases of our element polynomial spaces are made of monomials. However, when integrating the load vector or the error, the numerical integration is performed by subtessellation, where each polyhedron is broken into a number of tetrahedra and we use the quadrature rules developed for that kind of element. Without monomials (i.e., without HNI), the computational complexity would grow one order of magnitude (in terms of $p + \Delta p$). In some cases that would make our method prohibitively expensive, so that we would not be able to use high-order approximations or elements with a large number of faces (which require higher Δp).

We restrict the numerical study to the Poisson model problem analyzed above. Although this paper derives theoretical findings for variational problems formulated in fractional Sobolev spaces, here we compute with the limit case only ($\epsilon = 0$).

8.2 Results

For all cases we use smooth non-polynomial manufactured solutions u_{exact} and Dirichlet boundary conditions on the whole boundary. To obtain the rest of the exact solution components we calculate $\sigma_{exact} = \nabla u_{exact}$ and get the traces $(\hat{u}_{exact}, \widehat{\sigma \cdot n}_{exact})$ by simple restriction on every face of the mesh skeleton. Of course the boundary condition will be given by $\hat{u}_{exact}|_{\partial\Omega}$. Finally, the right-hand side load is determined by $f = -\Delta u_{exact}$.

The norms used to evaluate the error are

$$\begin{split} & \text{Error in } u_h = \frac{\|u - u_h\|_{L^2(\Omega)}}{\|u_{exact}\|_{L^2(\Omega)}} \\ & \text{Error in } \sigma_h = \frac{\|\sigma_{exact} - \sigma_h\|_{L^2(\Omega)}}{\|\sigma_{exact}\|_{L^2(\Omega)}} \\ & \text{Error in } \hat{u}_h = \left(\sum_{\text{Face } f \subset \partial \mathcal{T}} h_f^{-1} \|\hat{u}_{exact} - \hat{u}_h\|_{L^2(f)}^2\right)^{1/2} \\ & \text{Error in } \widehat{\sigma \cdot n}_h = \left(\sum_{\text{Face } f \subset \partial \mathcal{T}} h_f \|\widehat{\sigma \cdot n}_{exact} - \widehat{\sigma \cdot n}_h\|_{L^2(f)}^2\right)^{1/2} \end{split}$$

Observe that the first two deliver relative errors, while the other two give absolute errors as they are mesh-dependent norms. The choice of such error metrics for the traces is mainly driven by the need of having a cheap way to evaluate it. However, the one for \hat{u} is picked since it scales in the same way as the Slobodeckij seminorm in the $H^{1/2}$ norm, but does not require a double integral like the latter. The error norm

for $\widehat{\sigma \cdot n}$ is intended to compensate the fact that we are making use of L^2 norms to estimate convergence that is naturally set in a weaker topology $(H^{-1/2})$.

In the following error convergence graphs, instead of considering the mesh size parameter h, we use the total number of degrees of freedom (DOF), because if we use a quasiuniform mesh we can assert that $h^{-3} \sim \text{Total DOF}$.

We present three sets of results, which let us explore the flexibility of the DPG methodology with nonconforming traces and polyhedral elements. First, we use structured meshes with four different element sizes and observe the numerical convergence for low and high order approximations. Second, we go for a more general polyhedral mesh, namely a Voronoi tessellation, and even with such irregular elements we see how the numerical solution improve with a finer mesh and a higher polynomial degree. The third result set is motivated by a more practical point of view. There, we first use a popular tetrahedral mesh generator, which delivers unstructured meshes for certain domain. In addition to using the simplicial partition per se, we also use the idea of element agglomeration (or aggregation) [2, 18] in order to obtain polyhedral elements. Moreover, we use the fact that all faces are triangular to construct globally continuous trace spaces. We can therefore compare the behavior of such meshes with both continuous and discontinuous traces (whether with or without agglomeration). The practicality lies in two facts: i) by agglomerating portions of a fine mesh, we reduce the number of degrees of freedom while keeping the detailed representation of the geometry; ii) the underlying submesh provides a shape-regular partition as the one we assume in our theoretical setting, and can be used for integration, visualization, and adaptive refinement or coarsening. Although adaptivity is beyond the scope of the present publication, it is a subject of interest for future research on DPG with polyhedral elements.

8.2.1 Results with structured meshes

Our first domain is $\Omega = (0,1)^3$ and the manufactured solution is

$$u_{exact}(x) = \exp(x_1 + x_2 + x_3).$$

Notice that the gradient of $u_{exact}(x)$ consists of three copies of $\exp(x_1 + x_2 + x_3)$ and that the load is $f(x) = -3 \exp(x_1 + x_2 + x_3)$.

Three families of meshes consisting of structured tetrahedra, cubes and truncated octahedra are utilized. The coarsest meshes considered in this initial example are presented in Figure 8.1. Each of those is reproduced 8 times and scaled down to a half its size. This process is repeated 3 times, so that we have four meshes in each family. The refined meshes made with truncated octahedra can be visualized in Figure 8.2. Notice that these polyhedral elements have 7 and 14 faces, including pentagonal and hexagonal faces.

For each mesh, we use polynomial orders p = 1, 2, 3, 4. However, the enrichment parameter Δp must vary according to the type of element, intuitively requiring a higher enrichment as the number of faces increase. Sample solution plots are shown in Figure 8.3, where the type of mesh, order of approximation and enrichment are reported. Using the error metrics given above, we plot the numerical error convergence

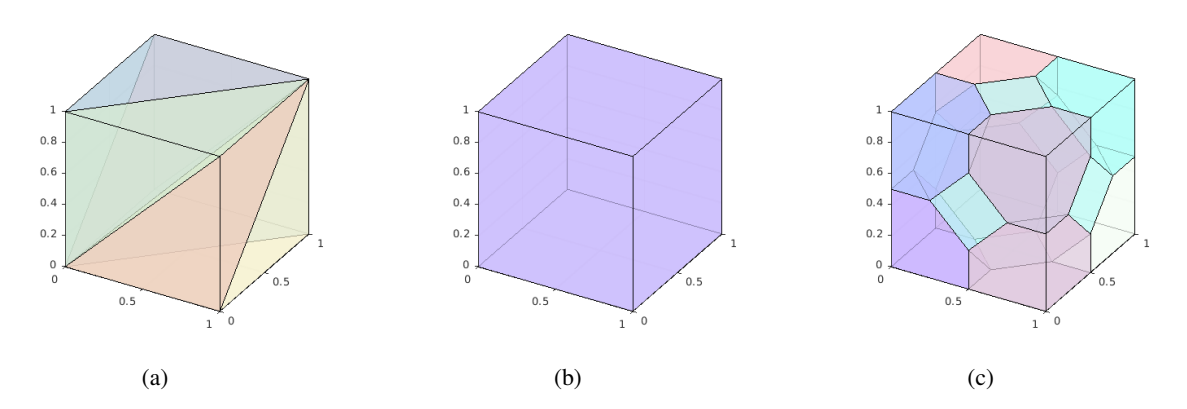


Figure 8.1: Coarse meshes for the first numerical study: (a) tetrahedra (6 elements), (b) cubes (1 element), (c) truncated octahedra (9 elements).

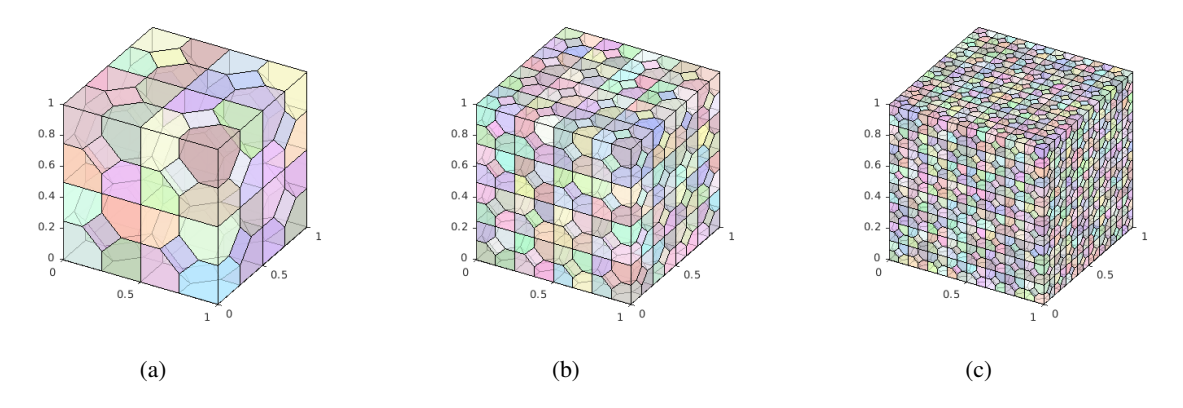


Figure 8.2: Fine truncated-octahedral meshes for the first numerical study: (a) 72 elements, (b) 576 elements, (c) 4608 elements.

for the three mesh families in Figures 8.4, 8.5 and 8.6. It is clear how the convergence is attained in all the mesh families and with the expected rates, for all the unknowns of the broken ultraweak formulation.

8.2.2 Results with Voronoi cells

For the second scenario we change the domain for $\Omega = (-1/2, 1/2)^3$ and keep the same manufactured solution. The meshes to be considered in this second study are generated through an algorithm called VoroCrust, which generates boundary-conforming Voronoi tessellations without clipping, even for complex 3D geometries (sharp features, multiple boundary components, non-watertight or non-manifold surfaces, etc.) [1].

In our current case we present meshes for the cube Ω , but as a result of VoroCrust, each element in the mesh is a real Voronoi cell, and all faces lying on the domain boundary are triangles. Because of the random sampling used in the meshing algorithm herein used, the cells in the partition may have a great number of neighbors (i.e., of faces). In Figure 8.7 we can visualize the exterior of a VoroCrust mesh and show the aspect of its interior elements. Some of those elements present over 40 faces, a feature that will demand a very high test space enrichment. Here, we report results of computations of our method over three different VoroCrust meshes, which consist of 204, 560 and 970 elements.

Polynomial orders p=1,2,3 are used with the Voronoi meshes, and the enrichment parameter is $\Delta p=6$ in most cases, although for p=3 the highest enrichment that we can compute with is $\Delta p=5$. It is an interesting result that we can observe convergence rates similar to the expected ones in the field variables only, while the trace variables are so poorly approximated that the error is orders of magnitude greater than with other meshes. Figure 8.8 includes sample plots of the numerical solution and error of one field variable, along with cut views of the resulting scalar field u_h . On this plane, the solution should be constant, so we see how the approximation improves when passing from the lowest order case to p=2. Finally, we show the error convergence graphs of u_h and σ_h in Figure 8.9. Notice how the convergence rate deteriorates as p=1 increases, which may be caused by insufficient enrichment of the local test spaces.

8.3 Results with unstructured tetrahedral meshes

The third setup uses another manufactured solution,

$$u_{exact}(x) = \sin(\pi x_1)\sin(\pi x_2)\sin(\pi x_3).$$

As for the domain herein used, we have again $\Omega = (-1/2, 1/2)^3$, but including an interface between two subdomains: a sphere of radius 1/4 and centered at the origin, and its complement in Ω . This is depicted in Figure 8.10(a). There is consequently a spherical surface that must be conformingly meshed. Even though we are not assigning different material properties to the subdomains, studying this geometric configuration will be of importance in many practical applications modelled with PDEs less simple than the Poisson equation. This geometry is meshed with NETGEN, a well-established unstructured tetrahedral mesh

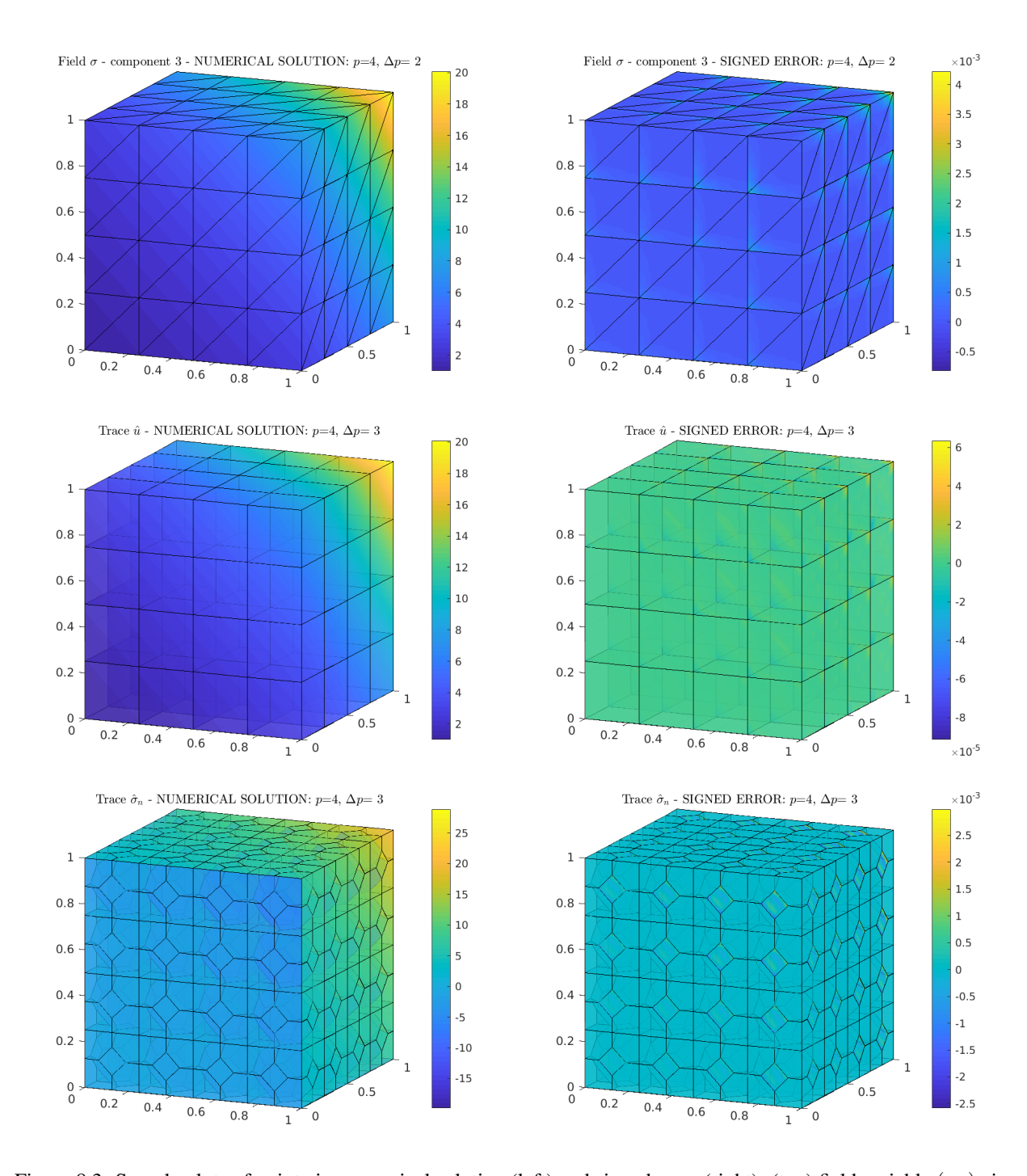


Figure 8.3: Sample plots of pointwise numerical solution (left) and signed error (right): (top) field variable $(\sigma_h)_3$ in a mesh of 384 tetrahedra, with p=4 and $\Delta p=2$; (middle) trace variable \hat{u}_h in a mesh of 64 cubes, with p=4 and $\Delta p=3$; (bottom) trace variable $\widehat{\sigma \cdot n}_h$ in a mesh of 576 truncated octahedra, with p=4 and $\Delta p=3$.

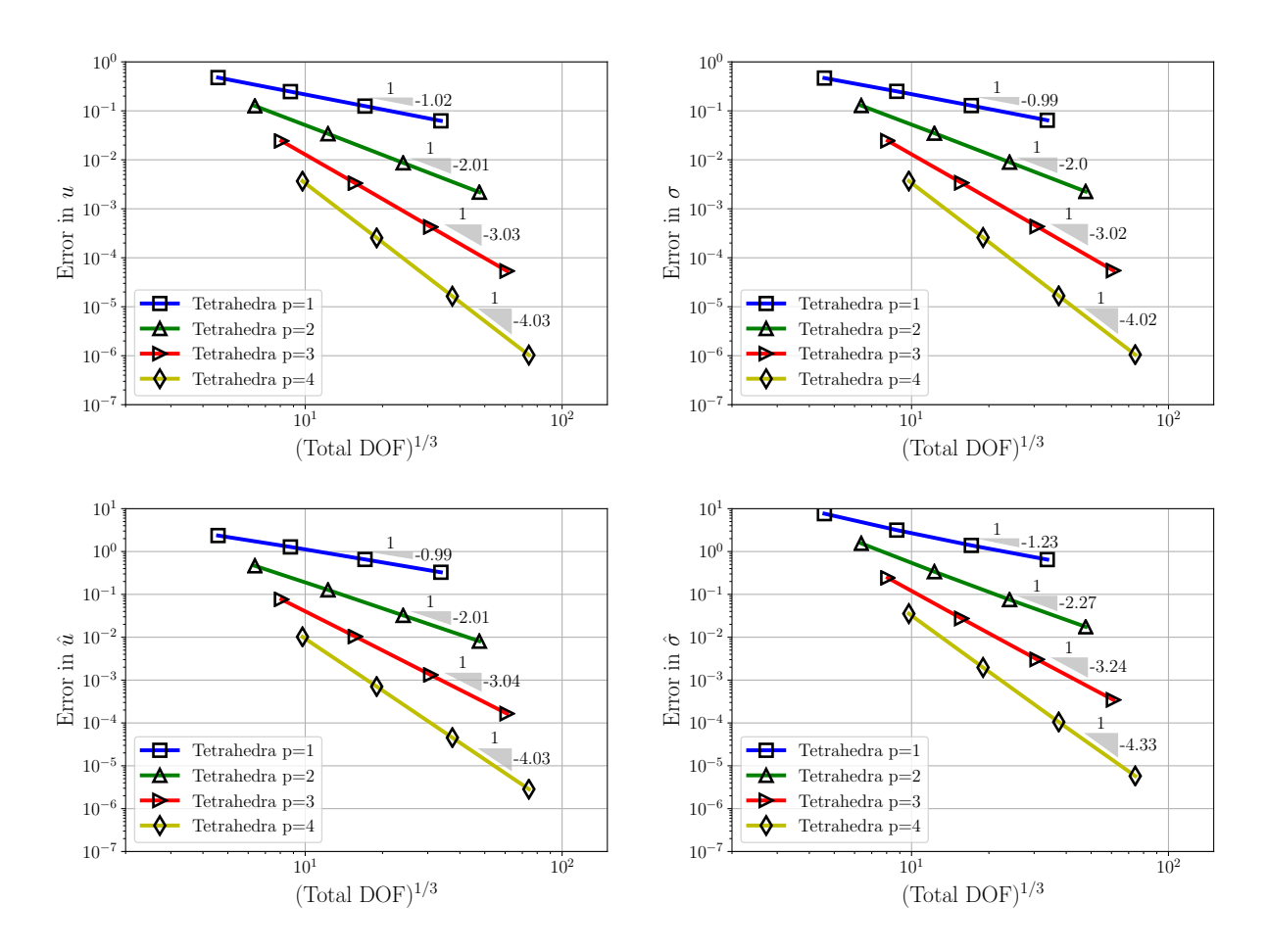


Figure 8.4: Error convergence in all variables for the tetrahedral mesh family and four polynomial orders. The enrichment parameter is $\Delta p = 2$.

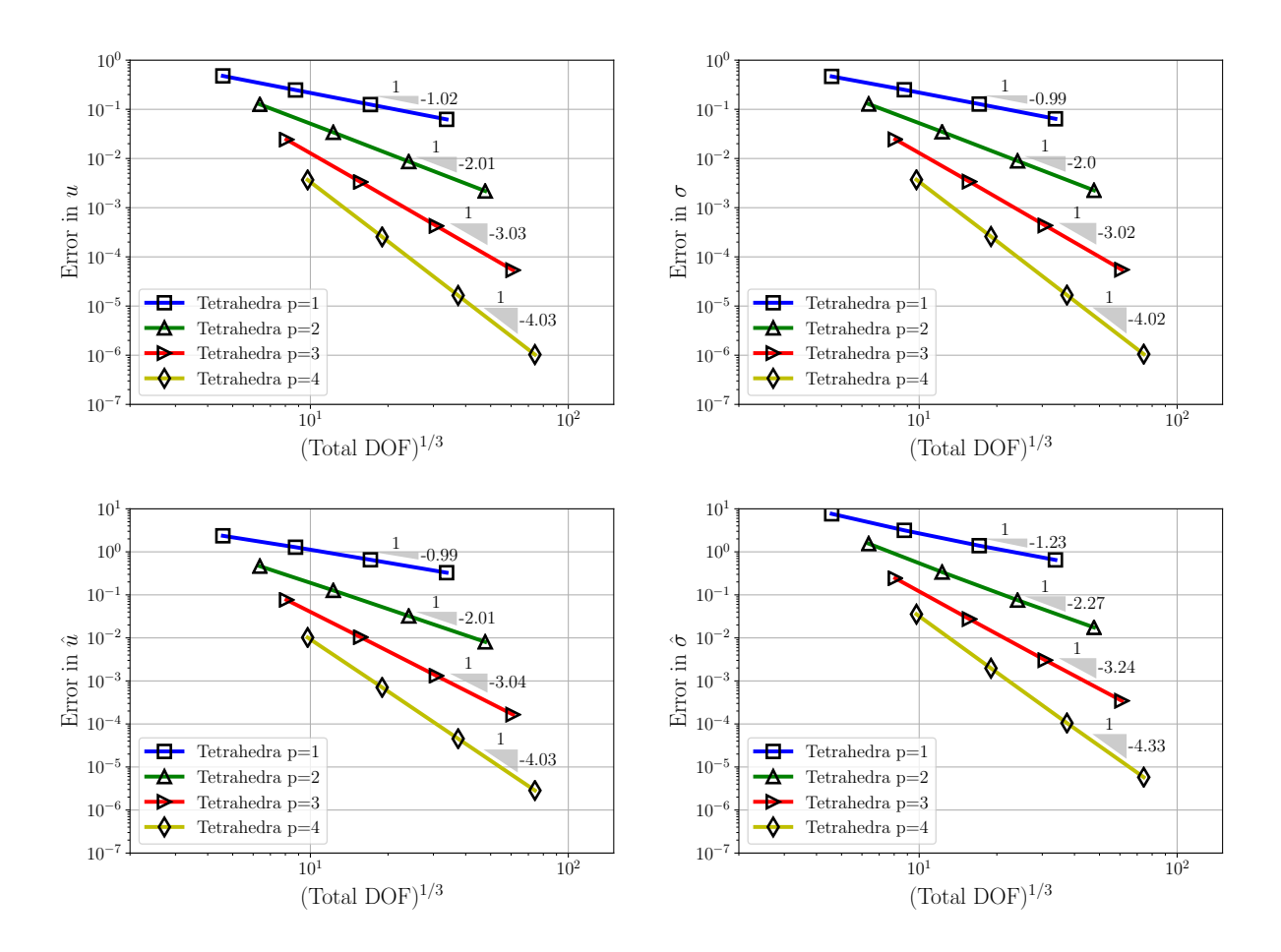


Figure 8.5: Error convergence in all variables for the cubic mesh family and four polynomial orders. The enrichment parameter is $\Delta p=3$.

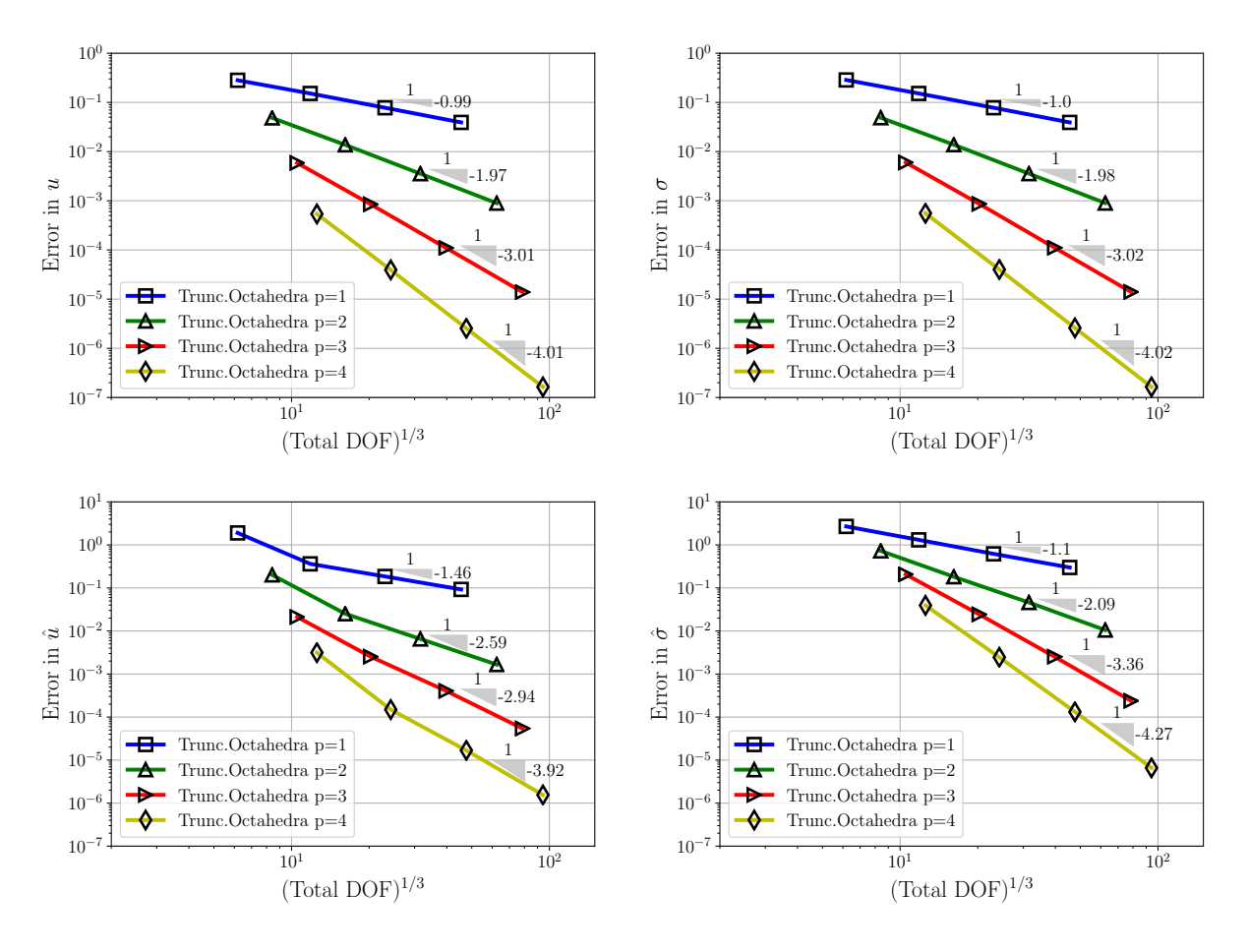


Figure 8.6: Error convergence in all variables for the truncated-octahedral mesh family and four polynomial orders. The enrichment parameter is $\Delta p = 3$.

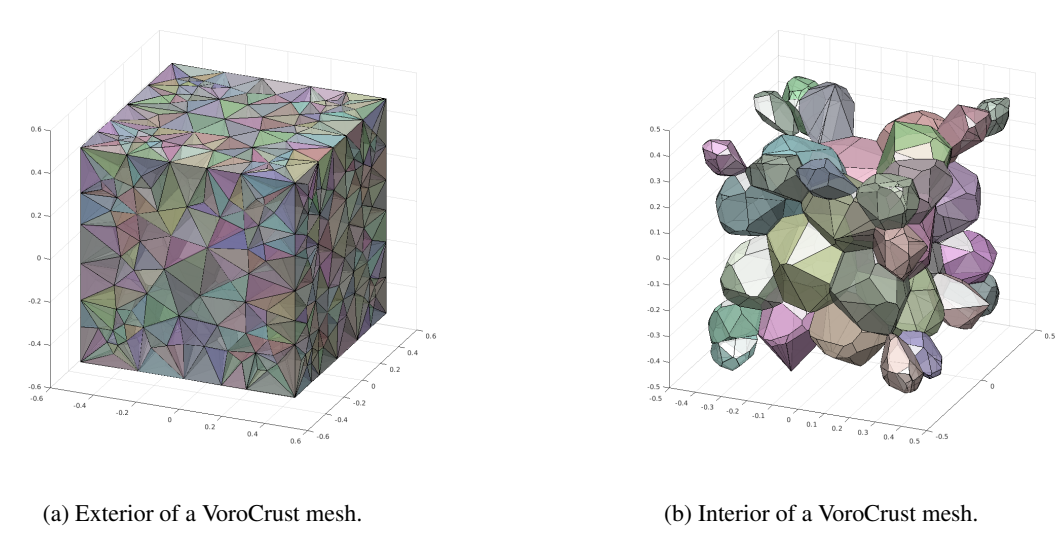


Figure 8.7: Polyhedral mesh generated with VoroCrust.

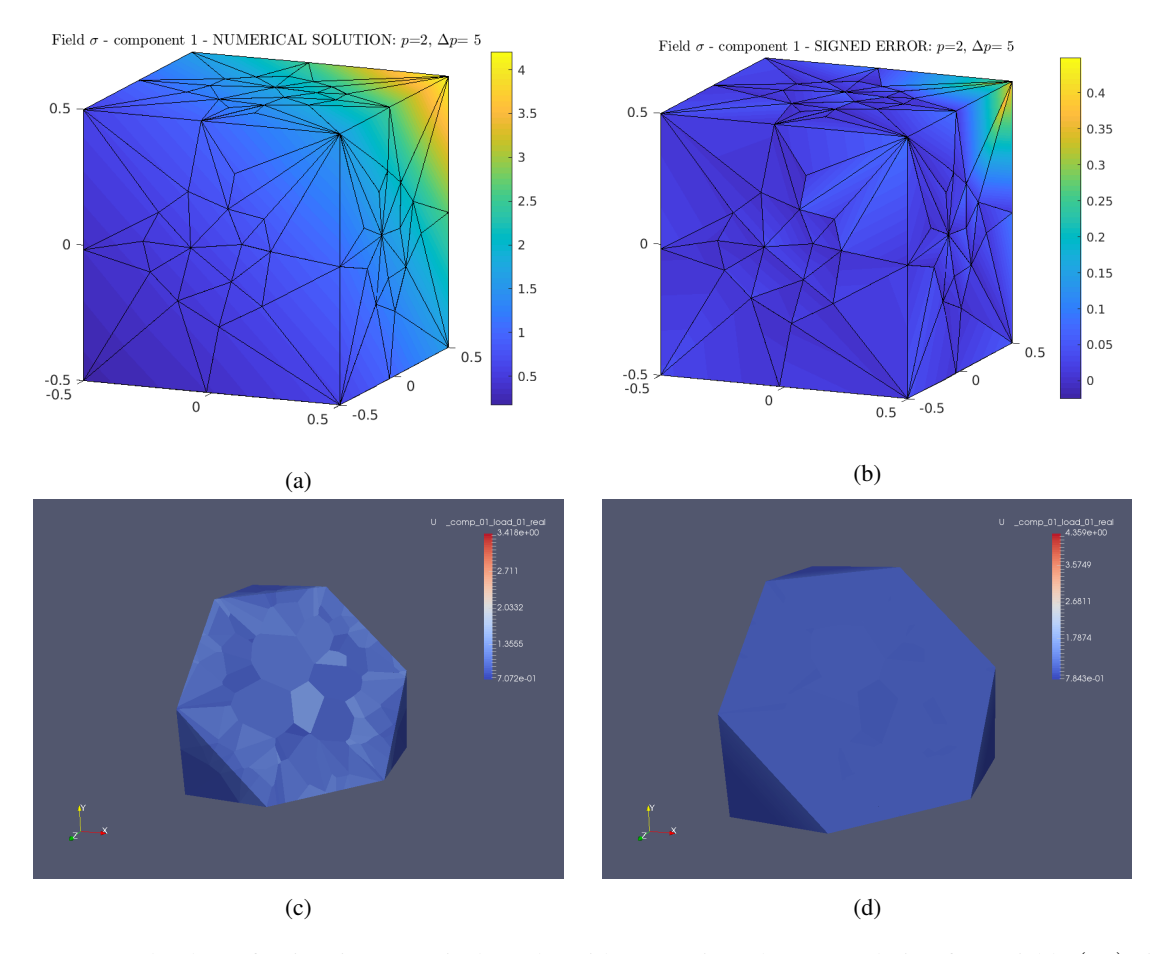


Figure 8.8: Sample plots of pointwise numerical results with Voronoi meshes: (a) solution for variable $(\sigma_h)_1$ in the 204-element Voronoi mesh with p=2, $\Delta p=6$; (b) signed error for variable $(\sigma_h)_1$ in the 204-element Voronoi mesh with p=2, $\Delta p=6$; (c) solution for variable u_h in a cut view of the 560-element Voronoi mesh with p=1, $\Delta p=6$; (d) solution for variable u_h in a cut view of the 560-element Voronoi mesh with p=2, $\Delta p=6$.

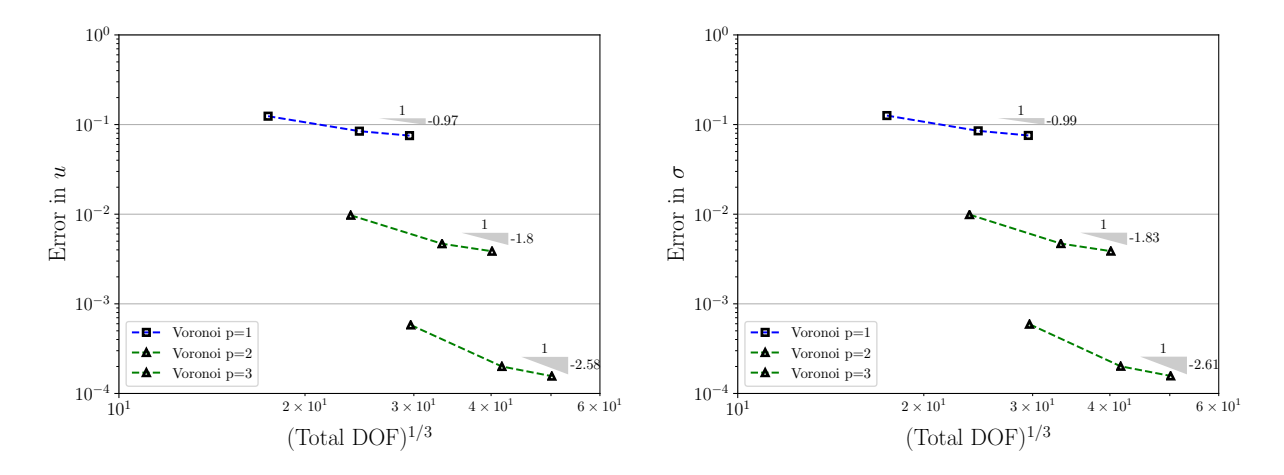


Figure 8.9: Error convergence in the field variables for the Voronoi mesh family and three polynomial orders.

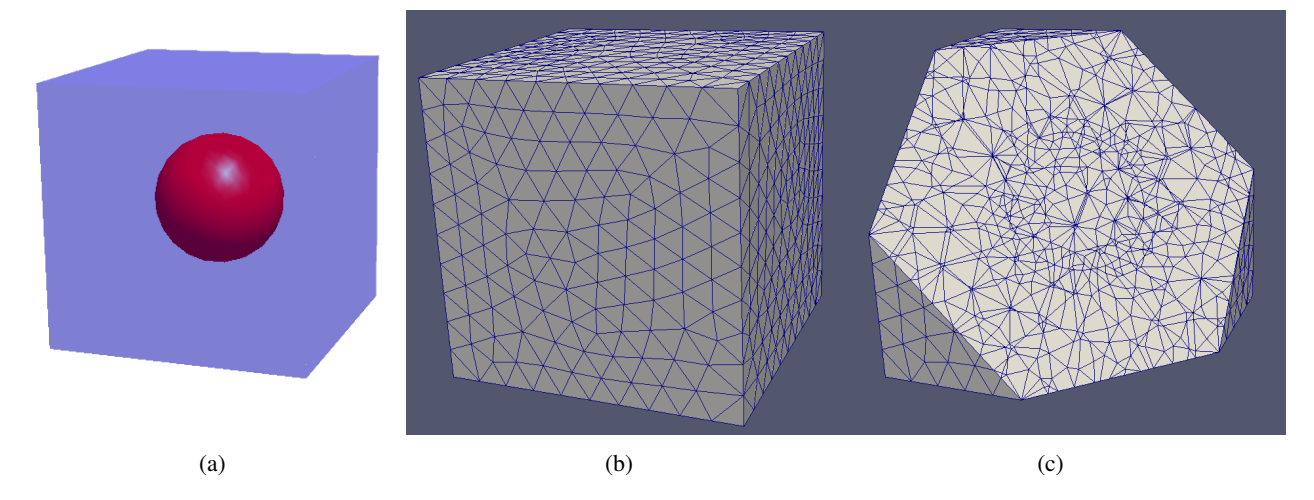


Figure 8.10: (a) The domain Ω showing an interior spherical surface that stands as the interface between two subdomains; (b) exterior of an unstructured 9462-element tetrahedral mesh of Ω ; (c) cut view of the mesh, where the conformity to the interior surface is visible.

generator (https://ngsolve.org/). Three meshes of 1545, 9462 and 27066 tetrahedra are obtained with this tool. The second of them can be appreciated in Figure 8.10(b),(c).

We run our method on these meshes for polynomial orders p=3,4,5. Sample plots of the numerical solution of both skeleton variables are presented in Figure 8.11.

Continuous traces Due to all faces being triangular, we can construct a globally continuous trace space for \hat{u}_h . For its implementation, we just need to know the relative orientation of edges with respect to faces to perform a modified assembly. However, all operations at the element level remain identical to the former procedure, save for a more careful evaluation of the face shape functions, as the orientations must be taken into account. For the meshes at hand, the enforcement of continuity of the trace makes this method a conforming finite element discretization, in the context of the broken ultraweak formulation. It can be regarded then as a conventional DPG discretization.

Plots in Figure 8.12 show the same variables as above, where small differences in the error can be observed, but most importantly the continuity of the numerical approximation to \hat{u} can be visualized. Figure 8.13 show convergence of all variables with these unstructured meshes, for both the continuous and the discontinuous discretization of the trace. It can be seen how enforcing continuity only saves relatively few DOF, while the error is almost identical to the solution with discontinuous traces. Notice how the case p=5 for the variable u_h initially experiences a great error decrease, but for the finest mesh, there is almost no improvement. We attribute such loss (in just 1 out of 4 unknowns) to numerical conditioning.

Element agglomeration The implementation of the element agglomeration approach is realized with the use of the graph-partitioning library METIS [37]. In order to have agglomerated elements that belong to

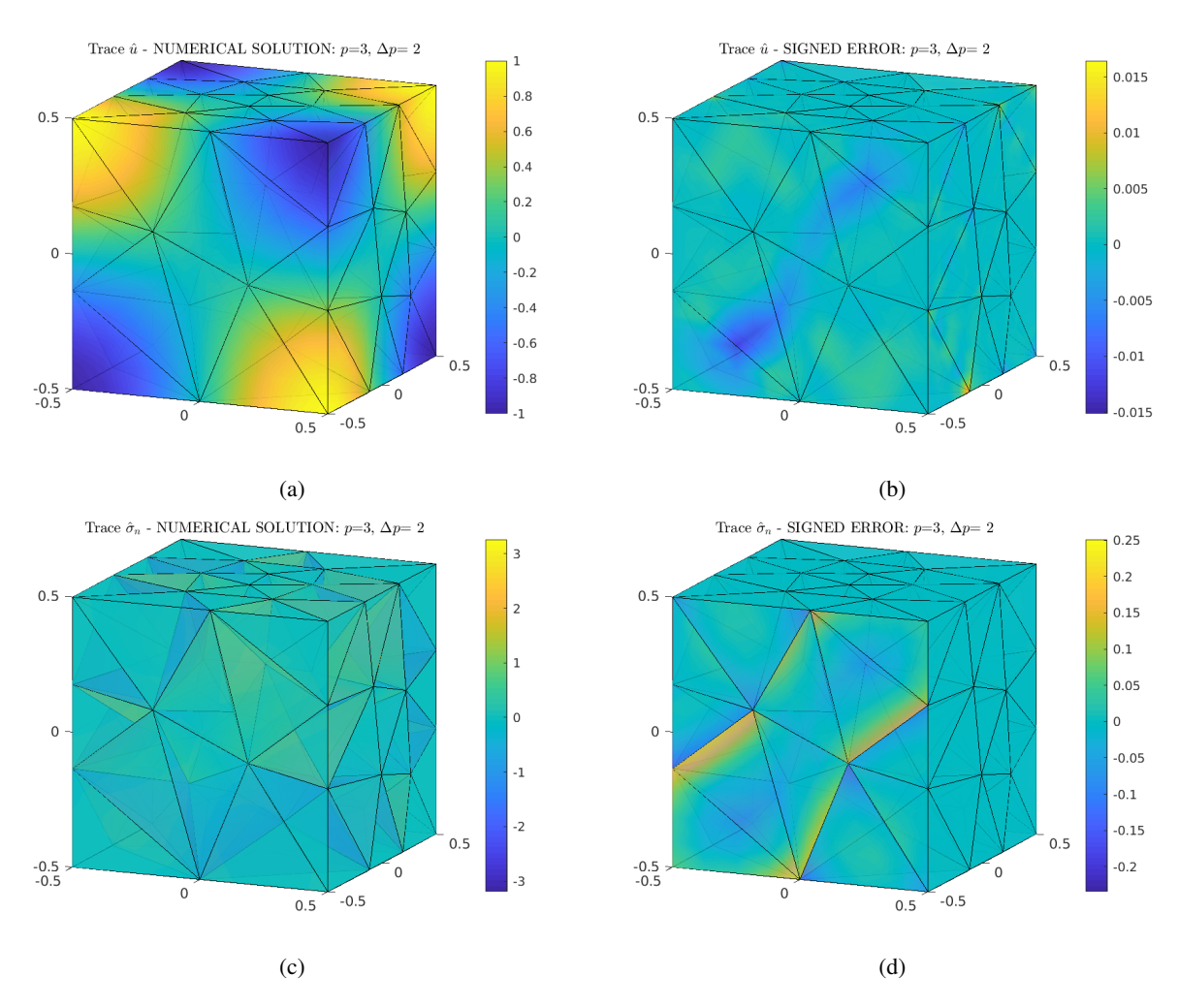


Figure 8.11: Sample plots of pointwise numerical solution (left) and signed error (right) in the 1545-element unstructured tetrahedral mesh, with p=3 and $\Delta p=2$: (top) variable \hat{u}_h ; (bottom) variable $\widehat{\sigma \cdot n}_h$.

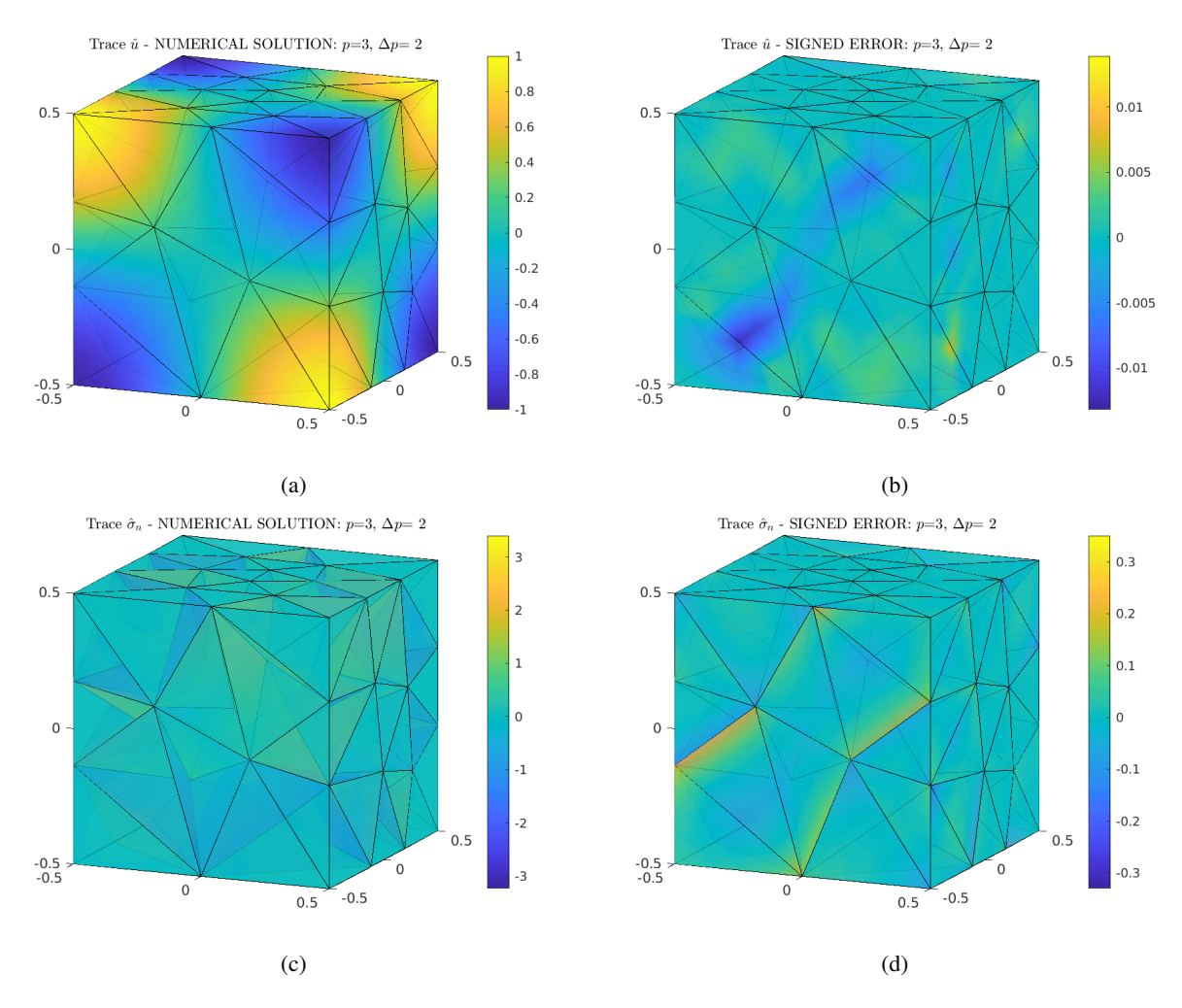


Figure 8.12: Sample plots of pointwise numerical solution (left) and signed error (right) in the 1545-element unstructured tetrahedral mesh **enforcing continuous discretization of trace** \hat{u} , with p=3 and $\Delta p=2$: (top) variable \hat{u}_h ; (bottom) variable $\widehat{\sigma \cdot n}_h$.

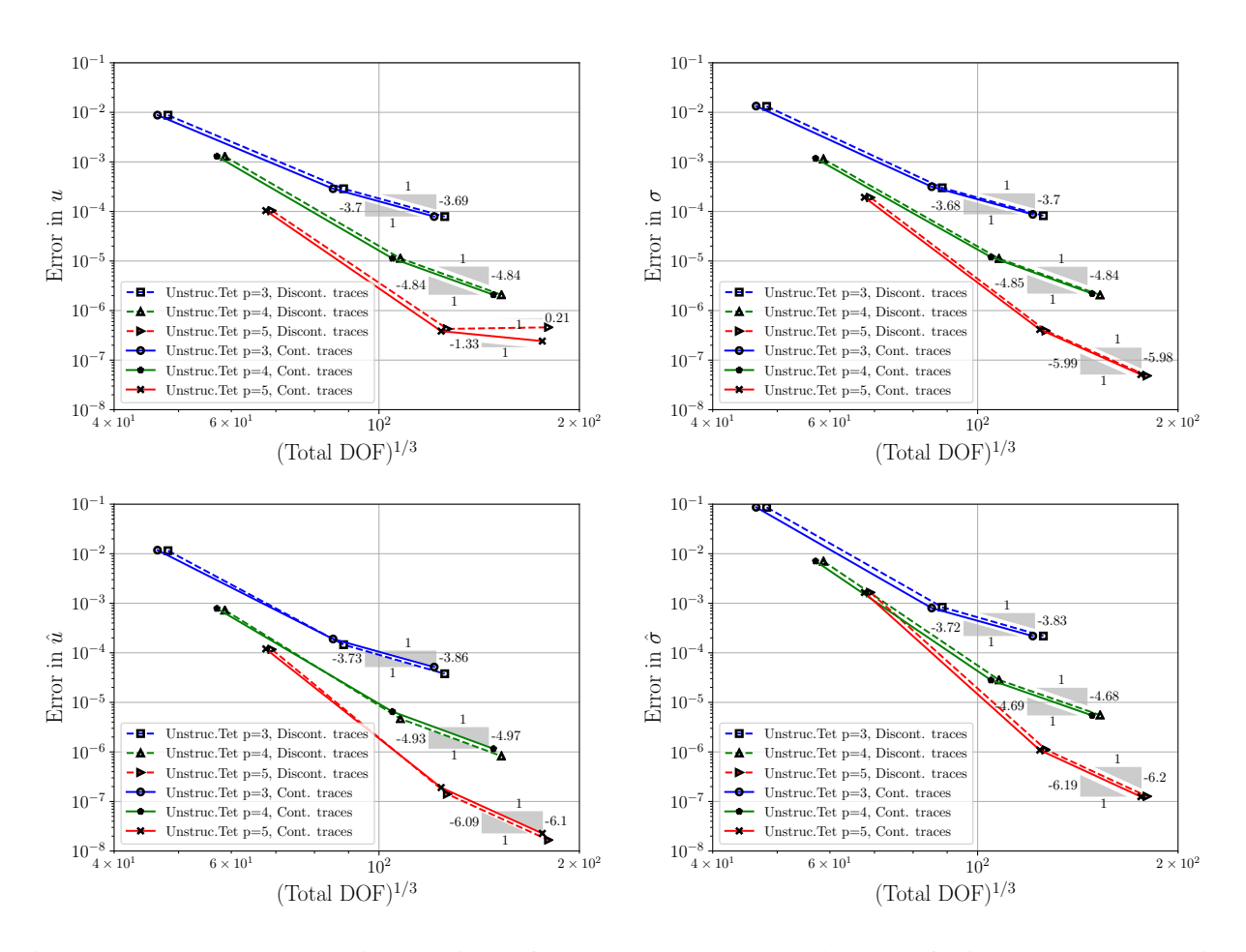


Figure 8.13: Error convergence in all variables for the unstructured tetrahedral mesh family and three polynomial orders, considering both discontinuous and continuous discretization of \hat{u} . The enrichment parameter is $\Delta p = 2$.

a single subdomain, the agglomeration process is performed on one subdomain at a time. It is possible to set the approximate number of tetrahedra per agglomeration, and here we use 16 and 64. Using this option delivers a very large number of faces per elements, since all triangles lying on the boundary of an agglomerated portion of the mesh is considered as an independent face, even if there are coplanar adjacent triangles. Using one of the unstructured tetrahedral meshes presented above, we apply the agglomeration algorithm and obtain meshes as the ones visualized in Figure 8.14.

During the computations it was noticeable that even though we have a large number of faces in any case, the enrichment parameter Δp may be lower when having continuous traces. A consequence of this is that we can raise p or agglomerate a greater quantity of tetrahedra when we enforce continuous traces. Sample plots of the numerical solution with p=3 are shown in Figure 8.15 with both discontinuous and continuous traces. Error convergence graphs for three variables are given in 8.16, including both types of trace discretization. There, only for the continuous trace scenario, we add two more series of results: the case p=4 in the same meshes (16 tetrahedra per element), and the case p=3 on a new set of meshes with 64 tetrahedra per element.

We can see in the error convergence plots for agglomerated elements that we have good rates, but because of the reduced amount of DOF, the magnitude of the error is still far from that of the original tetrahedral mesh, and the constant seems to be greater in the current setup. However, in the case p=4 we observe a significant advantage with respect to the other cases, and given that the rate is higher than 4, it rapidly reaches error levels that may be good enough for a practical problem.

A caveat for this approach was observed during the solving stage. We attribute such a major slowdown to the high number of faces that each element possesses, having to interact with many neighbors. This implies that the final DPG stiffness matrix is way less sparse than for elements with few faces, and the performance of the MUMPS solver gets therefore affected.

9 Conclusions

Acknowledgments. L. Demkowicz and J. Mora-Paz were partially supported with NSF grant No. 1819101 and a Sandia exploratory LDRD project (No. 19-1038, PI: Mohamed Ebeida). The first and last authors are grateful for an Oden Institute fellowship which allowed them to visit UT Austin in the Fall of 2019.

References

[1] Ahmed Abdelkader, Chandrajit L Bajaj, Mohamed S Ebeida, Ahmed H Mahmoud, Scott A Mitchell, John D Owens, and Ahmad A Rushdi. Vorocrust: Voronoi meshing without clipping. *arXiv preprint arXiv:1902.08767*, 2019.

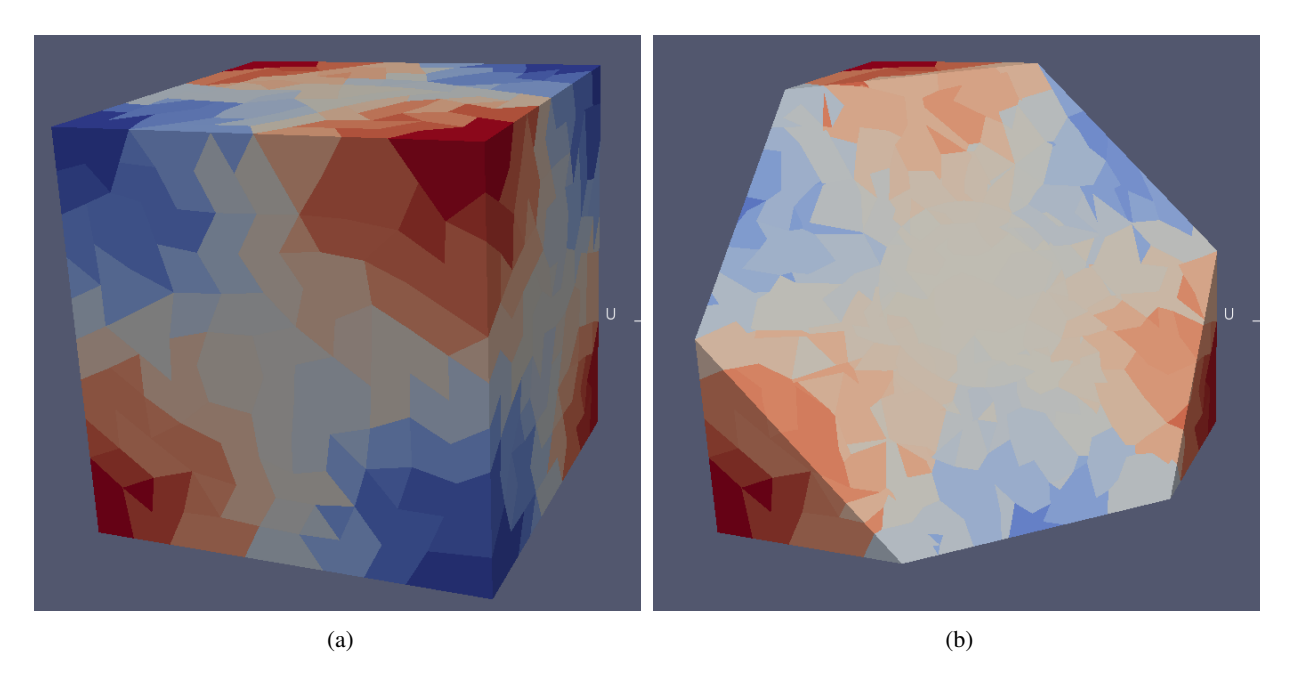


Figure 8.14: Agglomerated mesh, with about 16 tetrahedra per element: (a) exterior view, with each constant color representing a different element; (b) cut view showing that the agglomerated elements do not cross the subdomain interface.

- [2] Francesco Bassi, Lorenzo Botti, Alessandro Colombo, Daniele A Di Pietro, and Pietro Tesini. On the flexibility of agglomeration based physical space discontinuous galerkin discretizations. *J. Comput. Phys.*, 231(1):45–65, 2012.
- [3] L Beirão da Veiga, F Brezzi, A Cangiani, G Manzini, LD Marini, and A Russo. Basic principles of virtual element methods. *Math. Models Methods Appl. Sci.*, 23(01):199–214, 2013.
- [4] L Beirão da Veiga, F Brezzi, LD Marini, and A Russo. Virtual element method for general second-order elliptic problems on polygonal meshes. *Math. Models Methods Appl. Sci.*, 26(04):729–750, 2016.
- [5] Matias Fernando Benedetto, Stefano Berrone, Sandra Pieraccini, and Stefano Scialò. The virtual element method for discrete fracture network simulations. *Comput. Methods Appl. Mech. Engrg.*, 280:135–156, 2014.
- [6] J. E. Bishop. A displacement-based finite element formulation for general polyhedra using harmonic shape functions. *Int. J. Num. Meth. in Eng.*, 97(1):1–31, 2014.
- [7] Joseph E Bishop. Applications of Polyhedral Finite Elements in Solid Mechanics. In *Generalized Barycentric Coordinates in Computer Graphics and Computational Mechanics*, pages 179–196. CRC Press, 2017.
- [8] James H Bramble. *Multigrid methods*. CRC Press, 1993.

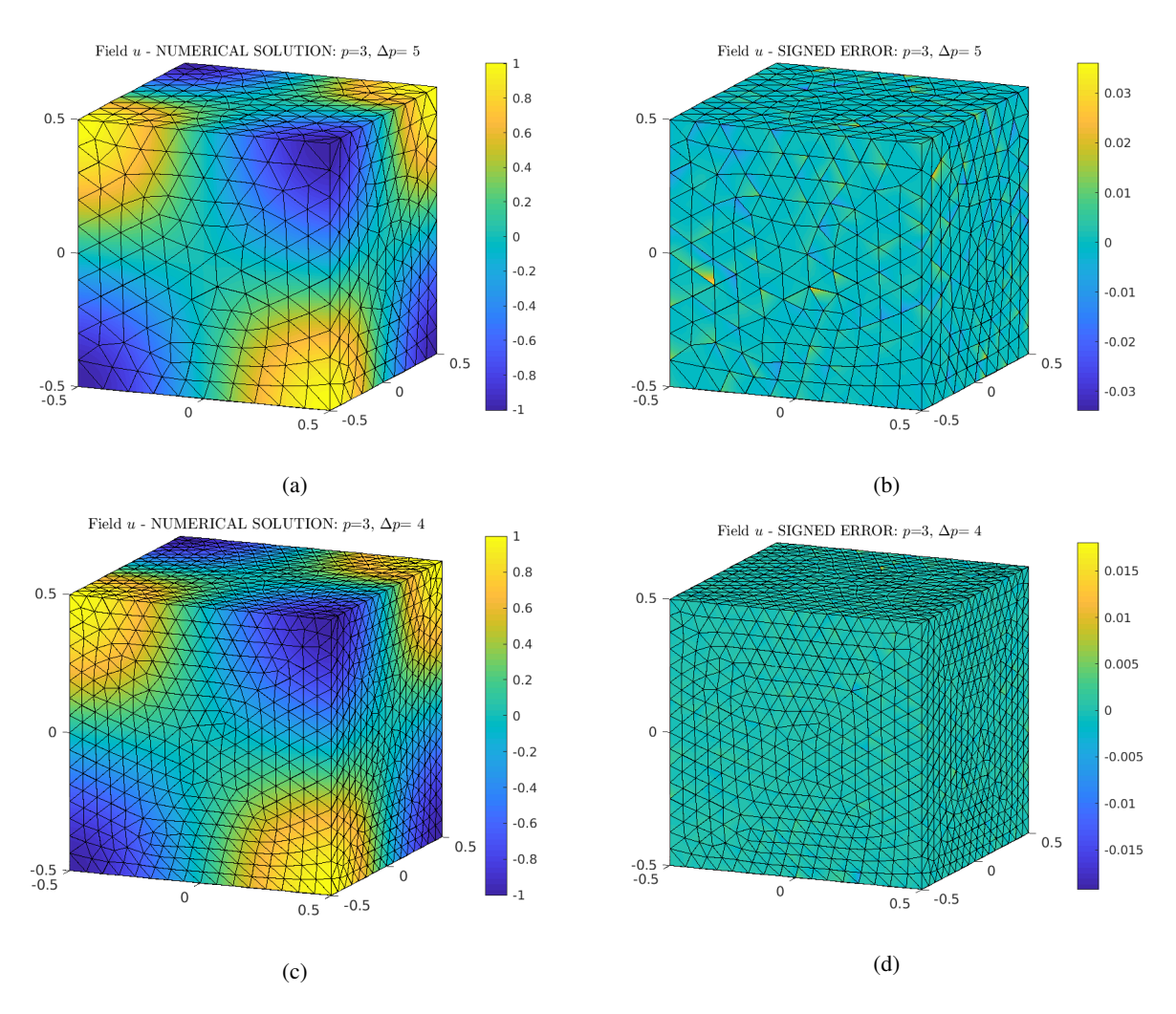


Figure 8.15: Sample plots of pointwise numerical solution (left) and signed error (right) for variable u_h in the agglomerated meshes of about 16 tetrahedra per element, with p=3: (top) underlying mesh of 9462 tetrahedra, with $\Delta p=5$ and **discontinuous** discrete trace \hat{u}_h ; (bottom) underlying mesh of 27066 tetrahedra, with $\Delta p=4$ and **continuous** discrete trace \hat{u}_h .

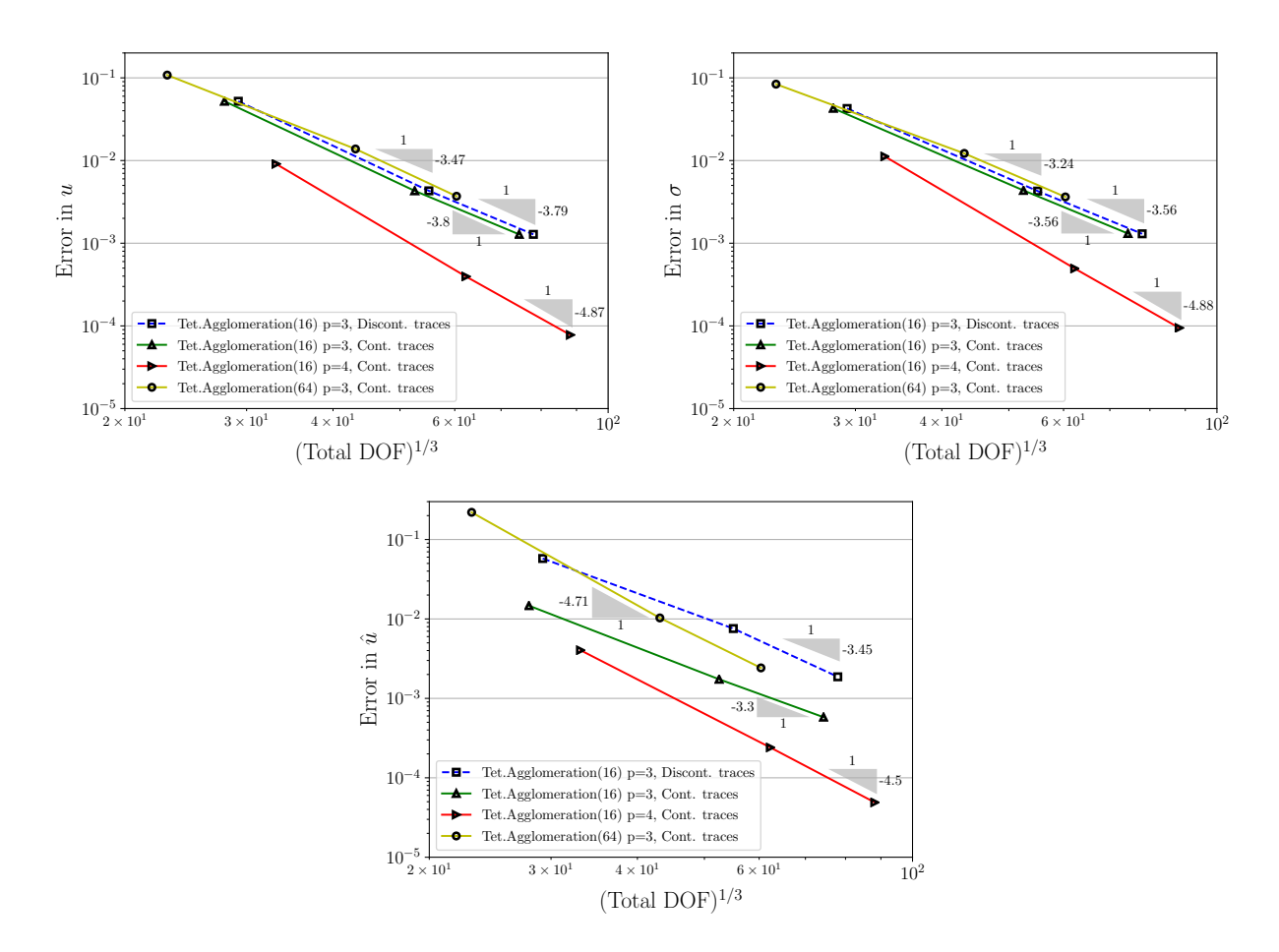


Figure 8.16: Error convergence in variables $(u_h, \sigma_h, \hat{u}_h)$ for the agglomerated mesh family and two polynomial orders, considering both discontinuous ($\Delta p = 5$) and continuous ($\Delta p = 4$) discretization of \hat{u} .

- [9] Franco Brezzi, Konstantin Lipnikov, and Valeria Simoncini. A family of mimetic finite difference methods on polygonal and polyhedral meshes. *Math. Models Methods Appl. Sci.*, 15(10):1533–1551, 2005.
- [10] Franco Brezzi and L Donatella Marini. Virtual element methods for plate bending problems. *Comput. Methods Appl. Mech. Engrg.*, 253:455–462, 2013.
- [11] Andrea Cangiani, Emmanuil H. Georgoulis, and Paul Houston. *hp*-Version discontinuous Galerkin methods on polygonal and polyhedral meshes. *Math. Models Methods Appl. Sci.*, 24(10):2009–2041, 2014.
- [12] C. Carstensen, L. Demkowicz, and J. Gopalakrishnan. Breaking spaces and forms for the DPG method and applications including Maxwell equations. *Comput. Math. Appl.*, 72(3):494–522, 2016.
- [13] Long Chen, Huayi Wei, and Min Wen. An interface-fitted mesh generator and virtual element methods for elliptic interface problems. *J. Comput. Phys.*, 334(1):327–348, 2017.
- [14] H Chi, L Beirão da Veiga, and GH Paulino. Some basic formulations of the virtual element method (VEM) for finite deformations. *Comput. Methods Appl. Mech. Engrg.*, 318:148–192, 2017.
- [15] Heng Chi, Cameron Talischi, Oscar Lopez-Pamies, and Glaucio H Paulino. Polygonal finite elements for finite elasticity. *Int. J. Num. Meth. in Eng.*, 101(4):305–328, 2015.
- [16] Eric B Chin, Jean B Lasserre, and N Sukumar. Numerical integration of homogeneous functions on convex and nonconvex polygons and polyhedra. *Comput. Mech.*, 56(6):967–981, 2015.
- [17] Bernardo Cockburn. Static condensation, hybridization, and the devising of the HDG methods. In Gabriel R. Barrenechea, Franco Brezzi, Andrea Cangiani, and Emmanuil H. Georgoulis, editors, *Build-ing Bridges: Connections and Challenges in Modern Approaches to Numerical Partial Differential Equations*, volume 114 of *Lecture Notes in Computational Science and Engineering*, pages 129–177. Springer, Cham, 2016.
- [18] Joe Collis and Paul Houston. Adaptive discontinuous Galerkin methods on polytopic meshes. In *Advances in Discretization Methods*, pages 187–206. Springer, 2016.
- [19] L Beirao da Veiga, F Brezzi, F Dassi, LD Marini, and A Russo. Virtual element approximation of 2d magnetostatic problems. *Computer Methods in Applied Mechanics and Engineering*, 327:173–195, 2017.
- [20] L Beirão Da Veiga, F Brezzi, LD Marini, and A Russo. H(div) and H(curl)-conforming virtual element methods. *Numer. Math.*, 133(2):303–332, 2016.
- [21] L Beirão Da Veiga, Franco Brezzi, and L Donatella Marini. Virtual elements for linear elasticity problems. *SIAM J. Numer. Anal.*, 51(2):794–812, 2013.

- [22] L. Demkowicz. Various variational formulations and Closed Range Theorem. Technical report, ICES, January 15–03.
- [23] L. Demkowicz. Lecture notes on Energy Spaces. Technical Report 13, ICES, 2018.
- [24] L. Demkowicz. Construction of DPG Fortin operators revisited. Technical Report 14, Oden Institute, August 2019.
- [25] L. Demkowicz and A. Buffa. H^1 , H(curl) and H(div)-conforming Projection-Based Interpolation in three dimensions. Quasi-optimal p-interpolation estimates. *Comput. Methods Appl. Mech. Engrg.*, 194:267–296, 2005.
- [26] L. Demkowicz and J. Gopalakrishnan. Analysis of the DPG method for the Poisson problem. *SIAM J. Num. Anal.*, 49(5):1788–1809, 2011. see also ICES Report 2010/37.
- [27] L. Demkowicz and J. Gopalakrishnan. *Recent Developments in Discontinuous Galerkin Finite Element Methods for Partial Differential Equations (eds. Xiaobing Feng, Ohannes Karakashian, Yulong Xing)*, volume 157, chapter An Overview of the DPG Method, pages 149–180. IMA Volumes in Mathematics and its Applications, 2014.
- [28] L. Demkowicz, J. Kurtz, D. Pardo, M. Paszyński, W. Rachowicz, and A. Zdunek. *Computing with hp Finite Elements. II. Frontiers: Three-Dimensional Elliptic and Maxwell Problems with Applications*. Chapman & Hall/CRC, October 2007.
- [29] L. Demkowicz, P. Monk, L. Vardapetyan, and W. Rachowicz. De Rham diagram for *hp* finite element spaces. *Comput. Math. Appl.*, 39(7-8):29–38, 2000.
- [30] Jérôme Droniou, Robert Eymard, Thierry Gallouët, and Raphaèle Herbin. A unified approach to mimetic finite difference, hybrid finite volume and mixed finite volume methods. *Math. Models Methods Appl. Sci.*, 20(2):265–295, 2010.
- [31] Johannes Ernesti and Christian Wieners. A space-time discontinuous petrov-galerkin method for acoustic waves. *Space-Time Methods. Applications to Partial Differential Equations*, pages 99–127, 2019.
- [32] F. Fuentes, B. Keith, L. Demkowicz, and S. Nagaraj. Orientation embedded high order shape functions for the exact sequence elements of all shapes. *Comput. Math. Appl.*, 70:353–458, 2015.
- [33] Arun L Gain, Glaucio H Paulino, Leonardo S Duarte, and Ivan FM Menezes. Topology optimization using polytopes. *Comput. Methods Appl. Mech. Engrg.*, 293:411–430, 2015.
- [34] Andrew Gillette, Alexander Rand, and Chandrajit Bajaj. Construction of scalar and vector finite element families on polygonal and polyhedral meshes. *Comput. Methods Appl. Math.*, 16(4):667–683, 2016.

- [35] J. Gopalakrishnan and W. Qiu. An analysis of the practical DPG method. *Math. Comp.*, 83(286):537–552, 2014.
- [36] N. Heuer, M. Karkulik, and F.-J. Sayas. Note on discontinuous trace approximation in the practical DPG method. *Comp. Math. Appl.*, 68:1562–1568, 2014.
- [37] George Karypis and Vipin Kumar. A fast and high quality multilevel scheme for partitioning irregular graphs. *SIAM Journal on scientific Computing*, 20(1):359–392, 1998.
- [38] Yu Kuznetsov, K Lipnikov, and M Shashkov. The mimetic finite difference method on polygonal meshes for diffusion-type problems. *Comput. Geosci.*, 8(4):301–324, 2004.
- [39] Jean Lasserre. Integration on a convex polytope. *Proceedings of the American Mathematical Society*, 126(8):2433–2441, 1998.
- [40] Jacques Louis Lions and Enrico Magenes. *Non-homogeneous boundary value problems and applications*, volume 1. Springer-Verlag, 1972.
- [41] Gianmarco Manzini, Alessandro Russo, and N Sukumar. New perspectives on polygonal and polyhedral finite element methods. *Math. Models Methods Appl. Sci.*, 24(08):1665–1699, 2014.
- [42] SE Mousavi and N Sukumar. Numerical integration of polynomials and discontinuous functions on irregular convex polygons and polyhedrons. *Comput. Mech.*, 47(5):535–554, 2011.
- [43] Lin Mu, Junping Wang, and Xiu Ye. Weak galerkin finite element methods on polytopal meshes. *arXiv* preprint arXiv:1204.3655, 2012.
- [44] S. Nagaraj, S. Petrides, and L. Demkowicz. Construction of DPG Fortin operators for second order problems. *Comput. Math. Appl.*, 74(8):1964–1980, 2017.
- [45] Milovan Peric and Stephen Ferguson. The advantage of polyhedral meshes. *Dynamics*, 24:45, 2005.
- [46] Alexander Rand, Andrew Gillette, and Chandrajit Bajaj. Quadratic serendipity finite elements on polygons using generalized barycentric coordinates. *Math. Comput.*, 83(290):2691–2716, 2014.
- [47] Daniel W Spring, Sofie E Leon, and Glaucio H Paulino. Unstructured polygonal meshes with adaptive refinement for the numerical simulation of dynamic cohesive fracture. *Int. J. Fract.*, 189(1):33–57, 2014.
- [48] A Tabarraei and N Sukumar. Application of polygonal finite elements in linear elasticity. *Int. J. Comput. Methods*, 3(04):503–520, 2006.
- [49] A Tabarraei and N Sukumar. Adaptive computations using material forces and residual-based error estimators on quadtree meshes. *Comput. Methods Appl. Mech. Engrg.*, 196(25):2657–2680, 2007.

- [50] Cameron Talischi, Glaucio H Paulino, Anderson Pereira, and Ivan FM Menezes. Polygonal finite elements for topology optimization: a unifying paradigm. *Int. J. Num. Meth. in Eng.*, 82(6):671–698, 2010.
- [51] Ali Vaziri Astaneh, Federico Fuentes, Jaime Mora, and Leszek Demkowicz. High-order polygonal discontinuous Petrov–Galerkin (PolyDPG) methods using ultraweak formulations. *Computer Methods in Applied Mechanics and Engineering*, 332:686–711, 2018.
- [52] E Wachspress. *A Rational Finite Element Basis*. Mathematics in Science and Engineering. Elsevier Science, 1975.

A Construction of Fortin Operators

Construction of $H(\operatorname{div})$ interpolation operator on master tetrahedron \hat{T} . Let $V^{p+1}(\hat{T})$ denote the Raviart-Thomas space of polynomials of order p+1 defined on master tetrahedron \hat{T} . We begin by recalling the construction of the Raviart-Thomas $H(\operatorname{div})$ interpolation operator.

$$\hat{\Pi}^{\text{div}}: H^{\epsilon}(\text{div}, \hat{T}) \to V^{p+1}(\hat{T}), \quad \tau \to \tau_{p}$$

$$\begin{cases} \langle (\tau_{p} - \tau) \cdot n, \phi \rangle = 0 & \forall \phi \in \mathcal{P}^{p}(f) \text{ for each face } f \text{ of } \hat{T} \\ (\tau_{p} - \tau, \psi) = 0 & \forall \psi \in \mathcal{P}^{p-1}(\hat{T}) \end{cases}$$
(A.47)

The operator commutes with the L^2 -projection onto $\mathcal{P}^p(\hat{T})$,

$$H^{\epsilon}(\operatorname{div}, \hat{T}) \xrightarrow{\operatorname{div}} H^{\epsilon}(\hat{T})$$

$$\downarrow \hat{\Pi}^{\operatorname{div}} \qquad \downarrow \hat{P}$$

$$V^{p}(\hat{T}) \xrightarrow{\operatorname{div}} \mathcal{P}^{p}(\hat{T}).$$

The finite-dimensionality argument implies that operator $\hat{\Pi}^{\mathrm{div}}$ is continuous on the space $H^{\epsilon}(\mathrm{div},\hat{T})$.

Construction of H(div) interpolation operator on an arbitrary tetrahedron. Let T be now an affine map from master tetrahedron \hat{T} onto an arbitrary tetrahedron T, $x = T\xi = A\xi + b$, $j = \det A$. We employ the standard Piola transforms for integer norms,

$$T_{\text{div}}: H(\text{div}, \hat{K}) \to H(\text{div}, K), \qquad \hat{\tau} \to \tau, \qquad \tau(x) = A\hat{\tau}(\xi)/j$$

 $T_{L^2}: L^2(\hat{K}) \to L^2(K), \qquad \qquad \hat{f} \to f \qquad f(x) = \hat{f}(\xi)/j$

The Raviart-Thomas interpolation operator defined on $H^{\epsilon}(\text{div}, K)$ is defined as follows,

$$P^{div}\tau := T_{\text{div}}\hat{P}^{\text{div}}\hat{\tau} = T_{\text{div}}\hat{P}^{\text{div}}T_{\text{div}}^{-1}\tau. \tag{A.48}$$

Let $P:L^2(T)\to \mathcal{P}^p(T)$ be the orthogonal projection. The use of the Piola transforms implies that

$$\operatorname{div} P^{div} \tau = P \operatorname{div} \tau = T_{L^2} \widehat{\operatorname{div}} \hat{\tau}.$$

Construction of H(div) Fortin operator for an arbitrary tetrahedron. We start by studying the scaling properties of the broken fractional norm for general elements:

$$\|\tau\|_{H^{\epsilon}(\mathcal{T}_h)}^2 := \sum_{K \in \mathcal{T}_h} \left(\|\tau\|^2 + |\tau|_{H^{\epsilon}(K)}^2 + \|\operatorname{div}\tau\|^2 + |\operatorname{div}\tau|_{H^{\epsilon}(K)}^2 \right) .$$

For a simple scaling, $x = h\xi + x_0$, using the Piola transform for L^2 -functions, we have,

$$||f||_{H^{\epsilon}(K)}^{2} = \int_{K} |f(x)|^{2} dx + \int_{K} \int_{K} \frac{|f(x) - f(y)|^{2}}{|x - y|^{3 + 2\epsilon}} dx dy$$

$$= h^{-3} \int_{\hat{K}} |\hat{f}(\xi)|^{2} d\xi + h^{-3 - 2\epsilon} \int_{\hat{K}} \int_{\hat{K}} \frac{|\hat{f}(\xi) - \hat{f}(\eta)|^{2}}{|\xi - \eta|^{3 + 2\epsilon}} d\xi d\eta$$

$$\leq h^{-3 - 2\epsilon} ||\hat{f}||_{H^{\epsilon}(\hat{K})}^{2}.$$

The result extends to general affine elements under standard shape regularity assumptions. Similarly, using the Piola transform for H(div)-space, we obtain

$$\|\tau\|_{H^{\epsilon}(K)}^2 \lesssim h^{-1-2\epsilon} \|\hat{\tau}\|_{H^{\epsilon}(\hat{K})}^2.$$

Now, assuming every element K corresponds to some tetrahedron T, the scaling properties imply the continuity of the Raviart-Thomas-Fortin operator:

$$\begin{split} \|\Pi^{\mathrm{div}}\tau\|_{H^{\epsilon}(T)}^2 &= \|T_{\mathrm{div}}\hat{P}^{\mathrm{div}}\hat{\tau}\|_{H^{\epsilon}(T)}^2 \lesssim h^{-1-2\epsilon}\|\hat{P}^{\mathrm{div}}\hat{\tau}\|_{H^{\epsilon}(\hat{T})}^2 \\ &\lesssim h^{-1-2\epsilon}\|\hat{P}^{\mathrm{div}}\|\,\|\hat{\tau}\|_{H^{\epsilon}(\hat{T})}^2 \lesssim h^{-2\epsilon}\|\hat{P}^{\mathrm{div}}\|\,\|\tau\|_{H^{\epsilon}(T)}^2 \\ \|\mathrm{div}\Pi^{\mathrm{div}}\tau\|_{H^{\epsilon}(T)}^2 &= \|P\mathrm{div}\tau\|_{H^{\epsilon}(T)}^2 \lesssim h^{-3-2\epsilon}\|\hat{P}\widehat{\mathrm{div}}\hat{\tau}\|_{H^{\epsilon}(\hat{T})}^2 \\ &\lesssim h^{-3-2\epsilon}\|\hat{P}\|\,\|\widehat{\mathrm{div}}\hat{\tau}\|_{H^{\epsilon}(\hat{T})}^2 \lesssim h^{-2\epsilon}\|\hat{P}\|\,\|\mathrm{div}\tau\|_{H^{\epsilon}(T)}^2 \,. \end{split}$$

where $\|\hat{P}^{\mathrm{div}}\|$, $\|\hat{P}\|=1$ are the norms of the Raviart-Thomas interpolation operator and L^2 -projection on the master element. Note that constant $\|\hat{P}^{\mathrm{div}}\|$ blows up with $\epsilon \to 0$ as the definition of operator for $\epsilon = 0$ is illegal. Combining the estimates, we obtain,

$$\|\Pi^{\operatorname{div}}\tau\|_{H^{\epsilon}(\operatorname{div},T)} \lesssim h^{-\epsilon}\|\hat{P}^{\operatorname{div}}\|\|\tau\|_{H^{\epsilon}(\operatorname{div},T)}. \tag{A.49}$$

Construction of H(div) and H^1 Fortin operators for an arbitrary polyhedron covered with a shape regular subelement tetrahedral mesh. Generalization of the construction discussed above to an arbitrary polyhedron depends strongly upon the definition of the enriched space which in turns depends clearly upon the number of faces. The choice of an appropriate polynomial enriched space and the construction of the corresponding Fortin operator are certainly challenging tasks.

We can collect though a "low hanging fruit". If the polyhedron can be covered with a shape-regular subelement tetrahedral mesh, we can employ the piecewise-polynomial $H(\operatorname{div})$ -conforming space of order p+1 defined on the tetrahedral submesh, and the corresponding discussed Raviart-Thomas interpolation

operator for the Fortin operator. Under the shape regularity for the submesh elements, the continuity properties remain intact. The operator satisfies the desired orthogonality properties for each subelement which implies that they are satisfied for the whole element as well.

The same idea applies to the H^1 Fortin operator. One can utilize any of the Fortin operators constructed in [35, 12, 44, 24] for the submesh elements.